

The SINC way: A fast and accurate approach to Fourier pricing

Fabio Baschetti* Giacomo Bormetti† Silvia Romagnoli‡
Pietro Rossi§¶

May 20, 2021

Abstract

The goal of this paper is to investigate the method outlined by one of us (PR) in Cherubini et al. (2009) to compute option prices. We name it the SINC approach. While the COS method by Fang and Osterlee (2009) leverages the Fourier-cosine expansion of truncated densities, the SINC approach builds on the Shannon Sampling Theorem revisited for functions with bounded support. We provide several results which were missing in the early derivation: i) a rigorous proof of the convergence of the SINC formula to the correct option price when the support grows and the number of Fourier frequencies increases; ii) ready to implement formulas for put, Cash-or-Nothing, and Asset-or-Nothing options; iii) a systematic comparison with the COS formula for several log-price models; iv) a numerical challenge against alternative Fast Fourier specifications, such as Carr and Madan (1999) and Lewis (2000); v) an extensive pricing exercise under the rough Heston model of Jaisson and Rosenbaum (2015); vi) formulas to evaluate numerically the moments of a truncated density.

The advantages of the SINC approach are numerous. When compared to benchmark

*Department of Statistics, University of Bologna, Italy E-mail: fabio.baschetti@studio.unibo.it

†Department of Mathematics, University of Bologna, Italy E-mail: giacomo.bormetti@unibo.it

‡Department of Statistics, University of Bologna, Italy E-mail: silvia.romagnoli@unibo.it

§Prometeia S.p.A., Bologna, Italy E-mail: pietero.rossi@prometeia.it

¶A previous version of this manuscript circulated with the title ‘Rough Heston: The SINC way’

methodologies, *SINC* provides the most accurate and fast pricing computation. The method naturally lends itself to price all options in a smile concurrently by means of Fast Fourier techniques, boosting fast calibration. Pricing requires to resort only to odd moments in the Fourier space.

Keywords: option pricing; rough Heston model; Fourier expansion; COS method; Fast Fourier methods

1 Introduction

The search of numerically efficient approaches to price options is the subject of intensive research. This fact comes with no surprise, since the ubiquitous presence and crucial role played by contingent claims in modern finance. It can be affirmed that, when the characteristic function (CF for short) of the log-price process is known in analytic or semi-analytic form, the current widely accepted solution to the pricing problem is the COS method by Fang and Oosterlee (2009). COS – a short-name for Fourier-cosine expansion – builds on the idea that it is computationally convenient to transform the expectation of the payoff with respect to the risk-neutral probability density function (PDF for short) into a linear combination of products of Fourier-cosine coefficients of the payoff and the density. To achieve this goal, the price to pay is the approximation of true PDF by a truncated version with bounded support, but the trick eventually reveals to be the crucial step to obtain an excellent pricing formula.

Our paper leverages the same idea of truncating the PDF, due to one of us (PR) and outlined in Cherubini et al. (2009), but from a different perspective. It exploits a well-known result which applies to periodic functions with limited bandwidth, i.e. the Shannon Sampling Theorem. The formal symmetry between the forward and backward Fourier transform readily provides the intuition that Shannon’s result can be adapted to functions with limited support in the direct space. As an interesting outcome of the application of the Sampling Theorem, one can express Plain Vanilla put and call prices, and digital

option constituents, as a Fourier-sinc expansion. Given that the sinc function is the Fourier transform of the rectangular function, it is not surprising that it may play a crucial role in representing expectations with respect to truncated densities. The convolution between the sinc function – which conveys the information related to the bounded support – and the Fourier transform of the Heaviside step function – which characterizes the point of discontinuity of the digital options – lends itself to analytic simplification by means of the Modified Hilbert transform. As a result, the option price can be represented as a series expansion which only requires the CF computation of the log-price process for odd moments. We refer to this method as *SINC approach*. As an important contribution, in this paper we prove in a rigorous way that the numerical error induced by the PDF truncation and by approximating a double infinite Fourier series by a finite sum can be made arbitrary small.

It is worth mentioning that both COS and *SINC* need to know the CF in order to be applied, hence this compulsory request singles out the range of applications we can deal with. The literature on stochastic models where it is natural to work in the Fourier space is huge and ever growing (see Cherubini et al. (2009) for an overview of the topic). The successful application of Fourier analysis to price options was pioneered by Chen and Scott (1992); Heston (1993); Bates (1996); Bakshi and Chen (1997); Scott (1997). The publication of Duffie et al. (2000) definitely celebrated the role of the transform analysis in dynamic asset pricing models when the state vector follows an affine jump-diffusion. The papers by Carr and Madan (1999) and Lewis (2000, 2001) contributed in a significant way to this stream of research in quantitative finance. In the former, the authors introduced a simple analytical expression for the Fourier transform of the option value, which allows to exploit the considerable computational power of the Fast Fourier Transform (FFT) in the inversion stage. The introduction of FFT techniques boosted the way to real-time calibration, pricing, and hedging. In the latter contributions, Lewis (2000, 2001) detailed a representation of the option price in terms of the CF which is rooted on a clever extension of the Fourier transform in the complex domain. His approach is naturally prone to the application of FFT, too. It is often preferred to the Carr and Madan (1999) approach, which requires the introduction of an auxiliary damping parameter. *SINC* is naturally

suitable for the computation by means of FFT. Then, not only *SINC* is based on a parsimonious representation of the option payoff, which requires to sample the CF at optimal points, but it expresses the payoff as a transform where the log-moneyness is the conjugate variable in the direct space. As a consequence, all option prices in a smile can be computed concurrently with $O(N \log_2 N)$ complexity, where N is the number of sample points in Fourier space, enhancing the computational advantage of *SINC* with respect to COS.

The stream of research inspired by the general framework introduced in Duffie et al. (2000) is vast. It ranges from models to equity and exchange rate option pricing, to interest rate derivative pricing, credit risk, and systemic risk modeling. Following (Fang and Oosterlee, 2009), first we test the performances of *SINC* on commonly used stochastic models for the equity log-price process, i.e. the Geometric Brownian motion (GBM), the Heston model (Heston, 1993), and the CGMY model by (Carr et al., 2002). Then, we focus on a restricted but stimulating and flourishing field, the modeling of financial volatility for pricing purposes ¹. The main reason of the interest in volatility modeling is that, recently, the celebrated Heston model has been revisited in several respects. Jaisson et al. (2015) showed that the Hawkes-based (Hawkes, 1971a,b) market microstructure model of Bacry et al. (2013) under nearly-unstable conditions converges in law to the Heston model. Jaisson et al. (2016) also proved that the microstructure model with an hyperbolic kernel by (Hardiman et al., 2013; Bacry et al., 2016) converges to an integrated fractional diffusion. The limiting process is very irregular, with a derivative behaving as a fractional Brownian motion with Hurst exponent smaller than 0.5 and close to zero. For this reason, it is dubbed rough Heston (rHeston for short). Gatheral et al. (2018) demonstrated for a wide range of assets that the historical volatility is rougher than a Brownian motion, and that the empirical moment of order q of the log-volatility increments are consistent with a scaling with Hurst exponent of order 0.1. Similar findings are reported in Bennedsen et al. (2016) under the historical measure, while Livieri et al. (2018) investigated the rough behavior of the implied volatility. Finally, contrary to classical volatility models, the rough

¹Monte Carlo methods represent an alternative approach to pricing under rough volatility. We do not consider it here, because it is quite aside from our main message. We refer the interested reader to (Bennedsen et al., 2017; McCrickerd and Pakkanen, 2018; Bayer et al., 2020) for recent developments.

ones (and so also the rHeston model) are able to reproduce the explosive behavior of the implied at-the-money (ATM) skew observed empirically when the option maturity goes to zero (Bayer et al., 2016; Fukasawa, 2011). Remarkably, El Euch and Rosenbaum (2019) derived a semiclosed formula for the CF of rHeston model. The formula is not fully explicit but given in terms of the solution of a fractional Riccati equation; the equation admits a unique continuous solution, whose closed form expression is unknown. To avoid the computational burden arising from the numerical solution of the fractional Riccati equation, in this paper we resort to the Padè approximant of the solution already discussed in Gatheral and Radoicic (2019). As shown by the authors, the rational approximation provides a very accurate description of the solution, especially for low values of the Hurst exponent H . In empirical investigations, both under the pricing and the historical measures, H is found to be of order 0.05-0.1, thus motivating the use of the rational approximation. An alternative approach is provided by the Adams scheme (Diethelm et al., 2004), possibly combined with a power series expansion and Richardson-Romberg extrapolation (Callegaro et al., 2020).

As a second main contribution of our paper, we challenge *SINC* against COS and *FFT-SINC* against Carr and Madan (1999) and Lewis (2000, 2001) approaches computed via FFT. Through extensive pricing under the forward variance specification, we assess the superiority in pricing accuracy of *SINC* with respect to competitors. The comparison is performed keeping the same number N_F of points sampled in the Fourier space equal for all methodologies. We believe this is the fairest way to claim the relative performance of the different algorithms, since the number of times the CF needs to be computed in rHeston represents the most time consuming step in pricing. Under this specification, when *SINC* is challenged against COS, the superiority of the former is apparent. When the full power of FFT is exploited, the numerical complexity reduction of *SINC* vs COS is sizable and dramatic, making *SINC* our preferred approach. As a matter of fact when dealing with the rHeston model, the main computational burden comes from the solution of the fractional Riccati equation needed to get the CF. This part greatly outweighs the cost of pricing

even a highly populated smile and the burden of using FT is twice as big as that of FFT in our exercise. Very much different is the case where the CF is known analytically; in that case the advantage of having a natural FFT formulation would be very large.

Last, but not least, as a side result of *SINC* approach, we detail in the Appendix a novel analytical methodology to approximate the moments of a random variable starting from the CF.

The remainder of the paper is organized as follows. In Section 2 we discuss the *SINC* formula and in Section 3 we characterize the numerical error. Sections 4 and 5 present the numerical results from the pricing exercise by means of the *SINC* and *FFT-SINC* specifications, respectively. Section 6 draws the most relevant conclusions. The Appendix provides technical details.

2 *SINC* at a glance

The *SINC* approach to price options is rooted on the following definition of a Fourier pair

$$\begin{aligned} g(x) &= \bar{\mathcal{F}}[\hat{g}(\kappa)] = \int_{\mathbb{R}} e^{-i2\pi x\kappa} \hat{g}(\kappa) d\kappa, \\ \hat{g}(\kappa) &= \mathcal{F}[g(x)] = \int_{\mathbb{R}} e^{+i2\pi x\kappa} g(x) dx, \end{aligned}$$

where $\bar{\mathcal{F}}$ and \mathcal{F} stand for the forward Fourier operator and the inverse Fourier operator, respectively and $g(\cdot)$ is integrable. Under the assumption of null interest rate and dividend yield, i.e. $r = 0$ and $q = 0$, it exploits the following decomposition of a Plain Vanilla (PV hereafter) put into Cash or Nothing (CoN hereafter) plus Asset or Nothing (AoN) options, i.e.

$$\mathbb{E}[(K - S_T)^+] = K\mathbb{E}[\mathbb{1}_{\{S_T < k\}}] - S_0\mathbb{E}[e^{s_T} \mathbb{1}_{\{S_T < k\}}], \quad s_T = \log\left(\frac{S_T}{S_0}\right), \quad k = \log\left(\frac{K}{S_0}\right) \quad (1)$$

with S_T and K denoting the underlying spot at time T and the exercise price, respectively ².

We note as $\theta(x)$ the Heaviside step function and recognize that contour integration yields

$$\theta(x) = \bar{\mathcal{F}}[\delta^-(\kappa)] = \int e^{-i2\pi\kappa x} \delta^-(\kappa) d\kappa,$$

where $\delta^-(\kappa) = \frac{i}{2\pi} \frac{1}{\kappa + i\varepsilon}$. In the Appendix (Section A), we recall the derivation of the previous result and clarify the role played by ε .

Therefore, if we write each of the expectations on the rhs of Equation (1) in terms of the PDF of the log-return s_T , $f(s_T)$, and the payoff of the option, we have that

$$\begin{aligned} \mathbb{E}[\mathbb{1}_{\{s_T < k\}}] &= \int f(s_T) \theta(k - s_T) ds_T = \bar{\mathcal{F}}[\mathcal{F}[f(k)] \mathcal{F}[\theta(k)]] = \bar{\mathcal{F}}[\hat{f}(\kappa) \delta^-(\kappa)] \\ &= \frac{i}{2\pi} \int e^{-i2\pi k \kappa} \hat{f}(\kappa) \frac{1}{\kappa + i\varepsilon} d\kappa, \end{aligned} \quad (2)$$

and

$$\mathbb{E}[e^{s_T} \mathbb{1}_{\{s_T < k\}}] = \int e^{s_T} f(s_T) \theta(k - s_T) ds_T = \frac{i}{2\pi} \int e^{-i2\pi k \kappa} \hat{f}\left(\kappa - \frac{i}{2\pi}\right) \frac{1}{\kappa + i\varepsilon} d\kappa \quad (3)$$

by simple means of the convolution theorem and the definition of a Fourier transform (FT for short).

Observe that a change of measure is implicit in the expectation defining the AoN put, which requires that $\mathbb{E}[e^{s_T}] = 1$.

For any given $\eta > 0$, we can find X_l and X_h for which

$$\left| 1 - \int_{X_l}^{X_h} f(s_T) ds_T \right| < \eta,$$

and the Shannon Sampling Theorem (Shannon, 1949) guarantees that the Fourier transform of the truncated function $f(s_T) \mathbb{1}_{X_l \leq s_T \leq X_h}$ can be fully recovered given a discrete (countable)

²The general formula for non zero interest rate and dividend yield is readily recovered by setting $s_T = \log(S_T/S_0) - (r-q)T$ and $k = \log(K/S_0) - (r-q)T$ and reads $\text{Put}(t=0, S_0) = e^{-qT} S_0 \mathbb{E}[(e^k - e^{s_T})^+]$.

set of points. Indeed, in the Appendix (Section B), we show that

$$e^{-i2\pi k\kappa} \overline{f \mathbb{1}_{\{X_l \leq s_T \leq X_h\}}}(\kappa) = \sum_{n=-\infty}^{\infty} e^{-i2\pi k\kappa_n} \overline{f \mathbb{1}_{\{X_l \leq s_T \leq X_h\}}}(\kappa_n) \text{sinc}[2\pi X_c(\kappa_n - \kappa)], \quad (4)$$

where $\kappa_n = n/(2X_c)$, $X_c = (X_h - X_l)/2$, and the sinc function is defined in the usual way as $\sin(x)/x$ (continuous at zero).

In other terms, the idea is that one can truncate the integration range in such a way that the contribution from the tails of the PDF is arbitrarily small, and getting rid of it provides an upper bound for the approximation error induced on the option price. As we are working with Fourier transforms, it is convenient to think of the length of the truncation range $2X_c$ as the periodicity of the bounded density. Then, we suggest that X_l and X_h are selected according to the following constraints

$$\int_{-\infty}^{X_l} f(s_T) ds_T < 10^{-10}, \quad \int_{-\infty}^{X_h} f(s_T) ds_T > 1 - 10^{-10}. \quad (5)$$

We will not allow for asymmetric intervals in our numerical sections and impose $X_h = -X_l = X_c$, for the sake of simplicity. Operationally, we compute the previous inequalities by means of Equation (9) and by choosing some safely large candidates for X_l and X_h , then define $X_c = 4 \max(|X_l|, |X_h|)$ and iterate until the difference between the new candidate value for X_c and the old one is less than 30%.

The need for truncating the density of the asset log-price is nothing new in the context of Fourier methods and it exactly motivates COS formulas by Fang and Oosterlee (2009). They in fact come up with one handy rule for determining the bounds of the PDF which reads as follows

$$[X_l, X_h] = \left[c_1 - L\sqrt{c_2 + \sqrt{c_4}}, c_1 + L\sqrt{c_2 + \sqrt{c_4}} \right]. \quad (6)$$

Here c_n tags the n -th cumulant of s_T and L is an arbitrary constant that mostly depends on the particular model one is considering. If this has the merit of being particularly simple, it still suffers from two problems: (i) it does not provide any clue as to the magnitude of the error associated with the truncation, and (ii) it requires knowledge of quantities which

are not always given in closed form (just think about the rHeston model, for example). The second limitation may be overcome by numerical evaluation of the moments of the distribution – we provide original formulas for doing so in the Appendix (Section E)– but the former is a very strong reason for preferring the cutting strategy we have described in the previous paragraph.

We will provide an explicit formula for the numerical evaluation of the cumulative distribution function (CDF) in (5) by the end of this section, and address to the numerical experiments for an assessment of its performance. It eventually turns out that the *SINC* is an excellent way to compute distribution functions, which fact makes our procedure for the bounds of the PDF particularly cheap. This may clearly be extended to the COS, but the evaluation of the CDF would be much more costly. In this regard, one may also observe that the periodicity of the PDF in the COS method is actually $4X_c$ but the support coincides with the *SINC*.

Now, we are in the position to recover both CoN and AoN put prices. Nevertheless, we only keep track of the CoN put for making things concise.³ As we have seen, bounding the PDF allows for an application of the Sampling Theorem: we plug Shannon’s representation (4) into the CoN Equation (2), straightforwardly write

$$\begin{aligned} \mathbb{E}[\mathbb{1}_{\{s_T < k\}}] &\simeq \mathbb{E}[\mathbb{1}_{\{s_T < k\}} \mathbb{1}_{\{X_l \leq s_T \leq X_h\}}] \\ &= \frac{i}{2\pi} \sum_{n=-\infty}^{\infty} e^{-i2\pi k \kappa_n} \overbrace{f \mathbb{1}_{\{X_l \leq s_T \leq X_h\}}(\kappa_n)}^{\text{}} \int \frac{\text{sinc}[2\pi X_c(\kappa_n - \kappa)]}{\kappa + i\varepsilon} d\kappa \end{aligned} \quad (7)$$

and finally recognize the inner integral in the sinc as a Modified Hilbert transform \mathcal{H}^- .

Definition 1. *The Modified Hilbert transform \mathcal{H}^- of a given function g is the result of a convolution of the distribution $\delta^-(x)$ with the function itself. This formally translates as:*

$$\mathcal{H}^- [g(y)] = \int g(y-x) \delta^-(x) dx = \frac{i}{2\pi} \int \frac{g(y-x)}{x+i\varepsilon} dx.$$

³The derivation of the AoN put price is perfectly equivalent to the CoN one. We decide to skip it because going through each steps would not add anything new.

In particular, the Appendix (Section C) proves that

$$\int \frac{\text{sinc}[2\pi X_c(\kappa_n - \kappa)]}{\kappa + i\varepsilon} d\kappa = \frac{2\pi}{i} \mathcal{H}^-[\text{sinc}(2\pi X_c \kappa_n)] = \frac{1}{2X_c \kappa_n} (1 - e^{i2\pi X_c \kappa_n}), \quad (8)$$

which is sufficient to specialize the CoN put as

$$\mathbb{E}[\mathbb{1}_{\{s_T < k\}}] \simeq \frac{i}{2\pi} \sum_{n=-\infty}^{\infty} e^{-i2\pi k \kappa_n} \widehat{f \mathbb{1}_{\{X_l \leq s_T \leq X_h\}}}(\kappa_n) \left[-i\pi \mathbb{1}_{n=0} + \frac{1 - (-1)^n}{n} \mathbb{1}_{n \neq 0} \right].$$

An additional approximation is introduced when truncating this last infinite sum to a finite (possibly low) number of terms and the price of the CoN option is written accordingly as

$$\mathbb{E}[\mathbb{1}_{\{s_T < k\}}] \simeq \frac{i}{2\pi} \sum_{n=-N/2}^{N/2} e^{-i2\pi k \kappa_n} \widehat{f \mathbb{1}_{\{X_l \leq s_T \leq X_h\}}}(\kappa_n) \left[-i\pi \mathbb{1}_{n=0} + \frac{1 - (-1)^n}{n} \mathbb{1}_{n \neq 0} \right].$$

Then the final formula follows replacing $\widehat{f \mathbb{1}_{\{X_l \leq s_T \leq X_h\}}}(\kappa_n)$ with $\hat{f}(\kappa_n)$ and recognizing that only the odd moments in the Fourier space are relevant for the computation

$$\mathbb{E}[\mathbb{1}_{\{s_T < k\}}] \simeq \frac{1}{2} + \frac{2}{\pi} \sum_{n=1}^{N/4} \frac{1}{2n-1} \left[\sin(2\pi k \kappa_{2n-1}) \Re[\hat{f}(\kappa_{2n-1})] - \cos(2\pi k \kappa_{2n-1}) \Im[\hat{f}(\kappa_{2n-1})] \right]. \quad (9)$$

Here \Re and \Im denote the real and imaginary parts, respectively. We show the validity of this final formula in the Appendix (Section D), and claim that the AoN option is priced in a very similar way, except that the CF needs to be evaluated for a complex argument, i.e.

$$\begin{aligned} \mathbb{E}[e^{s_T} \mathbb{1}_{\{s_T < k\}}] &\simeq \frac{i}{2\pi} \sum_{n=-N/2}^{N/2} e^{-i2\pi k \kappa_n} \hat{f}\left(\kappa_n - \frac{i}{2\pi}\right) \left[-i\pi \mathbb{1}_{n=0} + \frac{1 - (-1)^n}{n} \mathbb{1}_{n \neq 0} \right] \\ &= \frac{1}{2} + \frac{2}{\pi} \sum_{n=1}^{N/4} \frac{1}{2n-1} \left[\sin(2\pi k \kappa_{2n-1}) \Re\left[\hat{f}\left(\kappa_{2n-1} - \frac{i}{2\pi}\right)\right] \right. \\ &\quad \left. - \cos(2\pi k \kappa_{2n-1}) \Im\left[\hat{f}\left(\kappa_{2n-1} - \frac{i}{2\pi}\right)\right] \right]. \quad (10) \end{aligned}$$

Remark 1. *Out of the $N + 1$ terms that we included in the expansions, only $N/4$ survive. They correspond to the positive odd frequencies.*

While our cutting procedure provides us with explicit bounds on the PDF truncation error, we clearly need to control the impact of early termination of the infinite Fourier series and

the usage of the CF for the complete density in place of the reduced one. We consequently decompose the overall error as the sum of the three components described in Section 3 and study their behavior in the Appendix (Section F): each of them is bounded and the error shrunk under suitable choice of N and X_c , thus ensuring convergence of the *SINC* formulas to the true option price.

The puzzle is finally complete when we combine digital options to compute PV put prices:

Theorem 1. *Let \hat{f} denote the CF of the asset log-return $s_T = \log(S_T/S_0)$ and take $k = \log(K/S_0)$ the log-moneyness of the option. Then Equations (1), (9) and (10) justify the following writing of a PV put price*

$$\begin{aligned} \mathbb{E}[(K - S_T)^+] &\simeq \frac{1}{2}(K - S_0) \\ &+ \frac{2}{\pi} \sum_{n=1}^{N/4} \frac{1}{2n-1} \left[\sin(2\pi k \kappa_{2n-1}) \Re \left[K \hat{f}(\kappa_{2n-1}) - S_0 \hat{f}\left(\kappa_{2n-1} - \frac{i}{2\pi}\right) \right] \right. \\ &\quad \left. - \cos(2\pi k \kappa_{2n-1}) \Im \left[K \hat{f}(\kappa_{2n-1}) - S_0 \hat{f}\left(\kappa_{2n-1} - \frac{i}{2\pi}\right) \right] \right] \end{aligned} \quad (11)$$

where $\kappa_n = \frac{n}{X_h - X_l}$ and the interval $[X_l, X_h]$ is chosen so as to make the contribution from the tails of the PDF negligible.

To ease the interpretation of the results in the numerical sections and the comparison among different benchmark methodologies, we introduce the notation N_F to refer to the number of times the CF needs to be evaluated to compute the option price. For instance, to price a CoN put, it is sufficient to sample the CF $N_F = N/4$ times at points κ_{2n-1} ($N/4$ times at shifted points $\kappa_{2n-1} - i/(2\pi)$ for the AoN put) and to weight them with a suitable imaginary phase and the inverse of the integer odd numbers. The price of the PV put is readily recovered from AoN and CoN, thus by means of $N_F = N/2$ valuations of the CF. In the next sections, we are going to support the computational effectiveness of the *SINC* formulas, by challenging them against the COS ones and showing how the *SINC* approach can be readily adapted to the FFT framework.

2.1 The FFT form of *SINC*

One merit of *SINC* is that it is readily adapted to the stiff structure of the FFT algorithm. The computational speed of the Fast Fourier Transform is crucial for any concrete application within the calibration process and the extension comes with almost no effort in our setting.

We work under the assumption to price a discrete grid of strikes $k_m = m \frac{2X_c}{N}$, $-N/2 \leq m < N/2$ and to fit the remaining points, when needed, by linear interpolation from bucket to bucket.

Digital put prices at the aforementioned vector of strikes are now calculated as follows

$$\begin{aligned} \mathbb{E}[e^{asT} \mathbb{1}_{\{sT < k_m\}}] &\simeq \frac{i}{2\pi} \sum_{n=-N/2}^{N/2} e^{-i2\pi k_m \kappa_n} \hat{f}\left(\kappa_n - a \frac{i}{2\pi}\right) \left[-i\pi \mathbb{1}_{n=0} + \frac{1 - (-1)^n}{n} \mathbb{1}_{n \neq 0} \right] \\ &= \frac{i}{2\pi} \sum_{n=0}^{N-1} e^{-i \frac{2\pi}{N} mn} q_n \end{aligned} \quad (12)$$

where

$$q_n = \begin{cases} \frac{\pi}{i} & n = 0 \\ \hat{f}\left(\kappa_n - a \frac{i}{2\pi}\right) \frac{1 - (-1)^n}{n} & n \in [1, \frac{N}{2}) \\ 0 & n = \frac{N}{2} \\ \hat{f}\left(\kappa_{n-N} - a \frac{i}{2\pi}\right) \frac{1 - (-1)^{n-N}}{n-N} & n \in (\frac{N}{2}, N-1] \end{cases} \quad (13)$$

and a takes value 0 or 1 for CoN and AoN options, respectively. Equation (12), taken together with the definition of q_n in (13), expresses the *SINC* formulas in a form which can be readily computed by means of FFT. The formula for the PV put follows as before.

Remark 2. *In spite of the fact that the index n runs from 0 to $N-1$, a closer inspection reveals that the computation of q_n only requires the evaluation of the CF at $N/4$ different frequencies. Indeed, all q_n for even n are identically zero.*

The described procedure generates prices for CoN and AoN digitals indexed by the strikes $n(2X_c/N)$. To recover the price for different strikes (not belonging to the grid) we perform

a linear interpolation. The interpolation error can be reduced by increasing the number of terms in the expansion or resorting to the fractional FFT (frFFT) framework.

3 Error Analysis

As already mentioned, and similarly to the COS method of Fang and Oosterlee (2009), there are three sources of error affecting the SINC formula: the approximation of the true PDF with a truncated density, the replacement of a double infinite sum with a finite sum, and the substitution of the Fourier coefficients for the truncated density with the Fourier transform of the true PDF valued at discrete points. To characterize in a quantitative way the three error components, we proceed as follows.

The error associated to our approach can be written as ⁴

$$\begin{aligned} \epsilon &= \int f(s_T)\theta(k - s_T) ds_T - \frac{1}{2} - \frac{i}{2\pi X_c} \sum_{n=-N/4}^{+N/4} e^{-i2\pi k\kappa_{2n-1}} \frac{\hat{f}(\kappa_{2n-1})}{\kappa_{2n-1}} \\ &= \int f(s_T)\theta(k - s_T) ds_T - \int_{-X_c}^{X_c} f(s_T)\theta(k - s_T) ds_T \\ &\quad + \int_{-X_c}^{X_c} f(s_T)\theta(k - s_T) ds_T - \frac{1}{2} - \frac{i}{2\pi X_c} \sum_{n=-N/4}^{+N/4} e^{-i2\pi k\kappa_{2n-1}} \frac{\hat{f}(\kappa_{2n-1})}{\kappa_{2n-1}}. \end{aligned}$$

Exploiting the fact that

$$\int_{-X_c}^{X_c} f(s_T)\theta(k - s_T) ds_T = \frac{1}{2} + \frac{i}{2\pi X_c} \sum_{-\infty}^{+\infty} e^{-i2\pi k\kappa_{2n-1}} \frac{\widehat{f\mathbb{1}_{\{-X_c \leq s_T \leq X_c\}}}(\kappa_{2n-1})}{\kappa_{2n-1}},$$

we can write

$$\begin{aligned} \epsilon &= \int f(s_T)\theta(k - s_T) ds_T - \int_{-X_c}^{X_c} f(s_T)\theta(k - s_T) ds_T \\ &\quad + \frac{i}{2\pi X_c} \sum_{-\infty}^{+\infty} e^{-i2\pi k\kappa_{2n-1}} \frac{\widehat{f\mathbb{1}_{\{-X_c \leq s_T \leq X_c\}}}(\kappa_{2n-1})}{\kappa_{2n-1}} - \frac{i}{2\pi X_c} \sum_{n=-N/4}^{+N/4} e^{-i2\pi k\kappa_{2n-1}} \frac{\hat{f}(\kappa_{2n-1})}{\kappa_{2n-1}} \\ &= \int f(s_T)\theta(k - s_T) ds_T - \int_{-X_c}^{X_c} f(s_T)\theta(k - s_T) ds_T \end{aligned}$$

⁴As done before for the pricing formula, we detail the case of CoN put options. Similar results for the AoN puts can be readily derived.

$$\begin{aligned}
& + \frac{i}{2\pi X_c} \sum_{|n| > N/4} e^{-i2\pi k \kappa_{2n-1}} \frac{\widehat{f \mathbb{1}_{\{-X_c \leq s_T \leq X_c\}}}(\kappa_{2n-1})}{\kappa_{2n-1}} \\
& + \frac{i}{2\pi X_c} \sum_{-N/4}^{+N/4} e^{-i2\pi k \kappa_{2n-1}} \frac{\widehat{f \mathbb{1}_{\{-X_c \leq s_T \leq X_c\}}}(\kappa_{2n-1}) - \hat{f}(\kappa_{2n-1})}{\kappa_{2n-1}}.
\end{aligned} \tag{14}$$

The PDF truncation error reads

$$\epsilon_1 \doteq \int f(s_T) \theta(k - s_T) ds_T - \int_{-X_c}^{X_c} f(s_T) \theta(k - s_T) ds_T,$$

where we introduce the same notation, ϵ_1 , used in Fang and Oosterlee (2009). The second and last components of the error in Equation (14), that we refer to with ϵ_2 and ϵ_3 to conform with the notation in Fang and Oosterlee (2009), are the error contributions due to the truncation of a double infinite Fourier series and the replacement of the Fourier coefficients of the truncated PDF with the Fourier transform of the true PDF, respectively.

Such a decomposition of the overall error is the starting point to prove that the *SINC* price converges to the true option price: technical reasons and assumptions essential for the proof are given in the Appendix (Section F), where we bound the magnitude for each of the components in Equation (14) and conclude that the error can be made arbitrarily small by increasing the number of Fourier modes N and the truncation range $[-X_c, X_c]$.

4 *SINC* at work

In this section, we perform numerical tests to assess the accuracy of the *SINC* approach. We price PV puts and their digital components separately and span over various maturities and moneynesses for both standard models (GBM, Heston, and CGMY) and the rHeston model of El Euch and Rosenbaum (2018). The idea is to compare *SINC* and COS methods along the directions of precision and convergence speed. The COS is the most used method within the class of FT-based techniques. This is due to the acknowledged performance both in speed and accuracy. It is therefore natural to use it as reference.

The results we will produce show that the *SINC* is often better than COS when computing call and put option prices. Always orders of magnitude better when dealing with digital options. Furthermore, *SINC* enjoys the non negligible advantage to be tailor made for the FFT, while the COS, as we know, does not have a straightforward transition. The consequences of this will be more extensively discussed in the following section, where we also compare the *SINC* with standard FFT methods.

While option prices in the Black-Scholes model have a closed-form solution to be used as a benchmark we need to produce one benchmark for the other models. We decided to use the average between high precision ($N_F = 2^{20}$) *SINC* and COS prices and to chop them if the two happen to have more than 10 decimal digits in common.

4.1 Geometric Brownian Motion (GBM)

We begin with the simple example of a GBM for the price process. Selected parameters are the same as in Fang and Oosterlee (2009)

$$S_0 = 1 \quad r = 0.1 \quad q = 0 \quad T = 0.1 \quad \sigma = 0.25$$

and nine different strikes are considered, $K = 0.80 : 0.10 : 1.40$. This will be common throughout the section.

Table 1 reports relative errors with respect to the Black-Scholes price for both *SINC* and COS at different values of N_F . PV (lhs) and CoN (rhs) put options are considered, here.

Then, two facts are immediately apparent from the table:

Fact 1: *SINC* and COS experience different convergence rates, in general, and the type of considered option (either PV or a digital one) is going to change the patterns;

Fact 2: once the PDF truncation error is controlled and made sufficiently small, relatively low N_F is needed for the sum $\epsilon_2 + \epsilon_3$ to become negligible. This makes the *SINC* candidate to be a very good approximation of the true option price.

Table 1: Relative errors over PV and CoN put options for *SINC* and COS at different values of N_F in the Black-Scholes model. Stars (*) mean that the price fully conforms with the benchmark (up to the number of digits of the benchmark itself), straight lines denote relative errors that are larger than 100%. [$T = 0.1$, $X_c = 2.0105$]

		PV put						CoN put							
		N_F						benchmark	N_F						benchmark
	K	20	40	60	80	100	120		20	40	60	80	100	120	
SINC	0.60	—	—	5e-03	5e-04	5e-04	5e-04	1.974722e-13	—	3e-06	3e-06	3e-06	3e-06	3e-06	1.726736e-11
COS		—	—	—	—	—	2e-04		—	—	—	—	4e-01	1e-04	
SINC	0.70	—	4e-01	1e-07	1e-08	2e-09	2e-09	2.301833e-08	2e-02	4e-11	1e-11	1e-11	1e-11	1e-11	1.473992e-06
COS		—	—	—	1e-02	2e-05	4e-09		—	—	—	2e-02	1e-05	3e-10	
SINC	0.80	—	3e-04	9e-11	2e-12	2e-12	2e-12	3.2130086e-05	2e-05	2e-15	6e-14	6e-14	6e-14	6e-14	0.0014334833
COS		—	2e-01	2e-03	1e-05	1e-08	3e-12		—	8e-01	9e-03	2e-05	9e-09	2e-13	
SINC	0.90	2e-01	5e-06	2e-13	5e-14	1e-14	1e-14	0.0023972816	6e-07	3e-15	6e-16	6e-16	6e-16	6e-16	0.0693682968
COS		5e-01	2e-02	1e-04	3e-07	2e-10	4e-14		4e-01	2e-02	2e-04	6e-07	2e-10	7e-14	
SINC	1.00	1e-02	7e-07	7e-14	*	*	*	0.0266495182	5e-08	*	*	*	*	*	0.4607202900
COS		1e-01	2e-03	2e-05	4e-08	2e-11	4e-15		2e-02	1e-03	2e-05	6e-08	5e-11	1e-14	
SINC	1.10	4e-03	2e-07	4e-15	1e-15	*	*	0.0949509784	3e-08	1e-16	*	*	*	*	0.9456809861
COS		6e-03	7e-04	2e-06	1e-08	6e-12	*		5e-02	1e-04	2e-05	3e-08	3e-11	6e-15	
SINC	1.20	2e-03	2e-08	2e-14	3e-15	*	*	0.1885055786	5e-08	2e-16	*	*	*	*	1.1723357082
COS		2e-02	4e-04	2e-06	2e-09	7e-13	1e-15		1e-02	3e-04	1e-05	5e-08	4e-11	5e-15	
SINC	1.30	4e-05	9e-08	3e-15	4e-16	1e-15	1e-15	0.2870818751	4e-08	*	2e-16	2e-16	2e-16	2e-16	1.2862729107
COS		4e-04	2e-04	2e-06	4e-09	3e-13	1e-15		3e-02	8e-04	1e-06	4e-08	4e-11	4e-15	
SINC	1.40	1e-03	6e-09	9e-15	6e-16	*	*	0.3860701385	3e-08	2e-16	*	*	*	*	1.3860485750
COS		6e-03	6e-06	1e-06	2e-09	1e-12	*		6e-04	1e-03	8e-06	3e-08	3e-11	3e-16	

With particular respect to Fact 1, indeed, it is clear that the *SINC* approach outperforms the COS when the stock price process follows a GBM. The convergence is much faster when dealing with PV put options on the left of Table 1 and the difference is even larger (far larger) when it comes to cash-or-nothing options on the right of the same table.

However, these figures are model-specific and cannot suffice to build up a complete idea about the convergence of the two methods. We therefore test them against other models in the following subsections and try to understand if we can extract something systematic about their convergence properties. In doing so, we take care that the models we select cover a large range of scenarios: from pure-diffusion models to infinite activity and rough volatility models.

4.2 The Heston model

Our second case of study is the celebrated Heston model. We report the dynamics of the price and volatility here to fix the notation:

$$\begin{aligned}dS_t &= S_t \sqrt{V_t} dB_t^S \\dV_t &= -\lambda(V_t - \bar{V}) + \eta \sqrt{V_t} dB_t^V, \quad \langle dB^S, dB^V \rangle_t = \rho.\end{aligned}$$

As with Fang and Oosterlee (2009), again, we use parameters

$$\begin{aligned}S_0 = 1 \quad r = 0 \quad q = 0 \quad T = \{0.1, 1\} \quad \lambda = 1.5768 \quad \eta = 0.5751 \\ \bar{V} = 0.0398 \quad V_0 = 0.0157 \quad \rho = -0.5711.\end{aligned}$$

Table 2 repeats the same analysis as before in the context of the Heston model (we only replace CoN with AoN options to show that the numbers are somehow invariant between the two). Expiration is in 0.1 years, again, and we still observe improved convergence for the *SINC* as opposed to the COS when dealing with put options. Once more, the difference is strikingly evident with digital options, where about four times as many evaluations of the CF are needed for the COS to replicate the same accuracy as the *SINC*.

We also consider the case $T = 1$ in Table 3 and observe that our considerations are basically unchanged regardless of the maturity of the option.

4.3 CGMY

As for infinite activity models we take CGMY as an example (recall that the Variance Gamma may be recovered as a special case). Given that parameter Y is reported to play a special role in Fang and Oosterlee (2009), we place ourselves in the exact same settings as they did, and select the following parameters for the model

$$S_0 = 1 \quad r = 0.1 \quad q = 0 \quad T = \{0.01, 1\} \quad C = 1 \quad G = 5 \quad M = 5 \quad Y = \{0.50, 1.50, 1.98\}.$$

We add the very short maturity $T = 0.01$ to shed light on the case of short-dated out-of-the-money options.

Table 2: Relative errors over PV and AoN put options for *SINC* and COS at different values of N_F in the Heston model. Stars (\star) mean that the price fully conforms with the benchmark (up to the number of digits of the benchmark itself), straight lines denote relative errors that are larger than 100%. [$T = 0.1$, $X_c = 2.0499$]

		PV put						AoN put							
		N_F						benchmark	N_F						benchmark
	K	64	128	192	256	384	512		64	128	192	256	384	512	
SINC	0.60	—	—	—	7e-01	*	*	0.0000000011	—	4e-02	*	*	*	*	0.0000000397
COS		—	—	—	—	2e-01	*		—	—	—	—	—	2e-02	
SINC	0.70	—	—	2e-02	2e-03	*	*	0.0000002363	4e-01	3e-04	*	*	*	*	0.0000077645
COS		—	—	—	1e-01	2e-03	*		—	—	—	2e-01	9e-04	2e-04	
SINC	0.80	—	8e-02	3e-03	6e-05	*	*	0.0000198699	1e-02	6e-06	*	*	*	*	0.0006241401
COS		—	3e-01	2e-02	1e-03	7e-06	*		—	7e-02	3e-02	1e-02	3e-04	4e-06	
SINC	0.90	2e-01	3e-03	8e-05	2e-06	*	*	0.0008057899	8e-04	6e-07	*	*	*	*	0.0235660667
COS		2e-01	9e-03	7e-04	7e-05	9e-07	*		3e-01	4e-02	5e-03	7e-04	2e-05	5e-07	
SINC	1.00	2e-03	7e-05	4e-06	9e-08	*	*	0.0163700005	1e-04	1e-08	3e-10	*	*	*	0.4171058741
COS		2e-02	1e-03	1e-04	1e-06	2e-07	4e-09		7e-02	5e-03	5e-04	1e-04	3e-06	8e-09	
SINC	1.10	8e-04	5e-06	6e-07	2e-08	*	*	0.1000685530	9e-06	2e-08	*	*	*	*	0.9951985550
COS		2e-04	9e-05	1e-05	2e-06	3e-08	*		2e-02	2e-03	2e-04	9e-06	5e-07	2e-08	
SINC	1.20	8e-04	2e-05	4e-07	9e-09	*	*	0.2000001223	2e-05	1e-08	*	*	*	*	0.9999906356
COS		1e-03	1e-05	5e-06	2e-07	3e-09	*		1e-03	1e-03	2e-05	2e-05	5e-07	1e-08	
SINC	1.30	1e-04	1e-05	3e-08	7e-09	*	*	0.3000000002	1e-05	7e-09	1e-10	*	*	*	0.9999999797
COS		5e-04	3e-05	1e-06	8e-08	4e-09	*		8e-03	4e-05	8e-05	2e-05	9e-08	9e-09	
SINC	1.40	4e-04	4e-06	6e-08	5e-09	*	*	0.4000000000	3e-06	6e-09	*	*	*	*	0.9999999999
COS		1e-04	1e-05	1e-06	2e-07	2e-09	*		8e-03	6e-04	6e-05	4e-06	1e-07	7e-09	

Let us start with the case $Y = 1.5$. We point the reader to Tables 4 and 5 so that he/she can realize that convergence of the methods follows similar patterns as we have commented for the GBM and the Heston model, with the usual distinction between PV and digital options.

Then, approaching the limit case $Y = 2$ does not introduce any issue (this was known with the COS method and *SINC* is no different). Tables 6 and 7 confirm this fact.

More involved is the case $Y = 0.5$. Long maturities cause no deviations from the story we have told so far: look at Table 8 to see this. As expected, pricing short maturity options gets more complicated. When we look at PV put options on the lhs of Table 9 we see that the situation hints for an advantage of the COS. Only in this case we find the *SINC* approach to exhibit poorer performance with respect to its competitor. Nevertheless, two things are worth noticing: (i) *SINC* gets back its superiority (although less marked) when considering digital options (see rhs of Table 9) and (ii) convergence is very slow for the COS

Table 3: Relative errors over PV and AoN put options for *SINC* and COS at different values of N_F in the Heston model. Stars (\star) mean that the price fully conforms with the benchmark (up to the number of digits of the benchmark itself), straight lines denote relative errors that are larger than 100%. [$T = 1$, $X_c = 12.1802$]

		PV put						AoN put							
		N_F						N_F							
	K	128	192	256	384	512	768	benchmark	128	192	256	384	512	768	benchmark
SINC	0.60	1e-01	1e-02	1e-03	4e-06	2e-07	\star	0.0020880117	6e-04	3e-06	7e-08	\star	\star	\star	0.0104586356
COS		8e-02	2e-02	1e-03	2e-05	1e-05	3e-07		4e-01	4e-02	3e-02	3e-03	4e-04	3e-06	
SINC	0.70	2e-02	4e-03	7e-04	3e-06	2e-07	\star	0.0053328699	4e-04	4e-07	9e-08	\star	\star	\star	0.0275972090
COS		1e-02	5e-03	2e-03	2e-04	8e-06	2e-07		2e-01	6e-02	1e-02	6e-04	2e-04	2e-07	
SINC	0.80	3e-02	8e-04	3e-04	2e-06	2e-08	\star	0.0123663875	2e-04	2e-06	7e-09	\star	\star	\star	0.0674328518
COS		3e-02	5e-04	1e-03	1e-04	1e-06	9e-08		1e-01	4e-02	1e-02	2e-04	2e-04	2e-06	
SINC	0.90	9e-03	9e-04	9e-05	1e-06	1e-08	\star	0.0270953177	2e-05	7e-09	5e-09	\star	\star	\star	0.1601233888
COS		3e-02	5e-04	1e-03	1e-04	9e-06	1e-07		2e-02	3e-02	1e-03	1e-04	4e-06	2e-07	
SINC	1.00	3e-03	6e-04	5e-07	5e-07	2e-08	\star	0.0578515543	6e-05	1e-06	2e-08	\star	\star	\star	0.3750835043
COS		9e-03	1e-03	8e-04	6e-05	3e-06	\star		6e-02	2e-02	3e-03	4e-04	6e-05	1e-06	
SINC	1.10	2e-03	9e-05	2e-06	3e-07	8e-09	\star	0.1178713500	5e-05	7e-07	6e-09	\star	\star	\star	0.7236745029
COS		8e-03	1e-03	2e-04	5e-06	6e-07	3e-08		4e-02	1e-02	4e-03	4e-04	5e-05	6e-07	
SINC	1.20	1e-03	1e-04	1e-05	1e-07	2e-10	\star	0.2048282813	3e-05	5e-07	7e-09	\star	\star	\star	0.9222278418
COS		6e-03	1e-03	6e-05	2e-05	3e-07	9e-09		8e-03	5e-03	3e-03	1e-05	3e-05	5e-07	
SINC	1.30	1e-03	1e-04	2e-05	2e-07	4e-09	\star	0.3014759365	2e-05	2e-07	2e-09	\star	\star	\star	0.9771415014
COS		2e-03	8e-04	8e-05	7e-06	7e-07	1e-08		2e-02	2e-03	2e-03	2e-04	2e-05	3e-07	
SINC	1.40	9e-04	9e-05	2e-06	1e-07	3e-09	\star	0.4005141485	5e-06	2e-07	4e-09	\star	\star	\star	0.9922869299
COS		2e-03	5e-07	1e-04	1e-06	7e-07	3e-09		9e-03	6e-03	1e-03	2e-04	4e-06	3e-07	

as well as a result of enormously peaked density for the asset log-price. We plot the PDF for a CGMY process with $C = 1, G = 5, M = 5, Y = 0.5$ and maturity $T = 1, T = 0.01$ in Figure (1). Plotting the PDF is both very simple and computationally convenient when using the *SINC* approach. The duality of the PDF and the CF is the theoretical backbone behind our procedure and the FT/FFT/frFFT provide the numerical tools for Fourier inversion.

We have the following obvious fact:

Fact 3: the number of evaluations of the CF that guarantees convergence to the benchmark increases with peaked density functions.

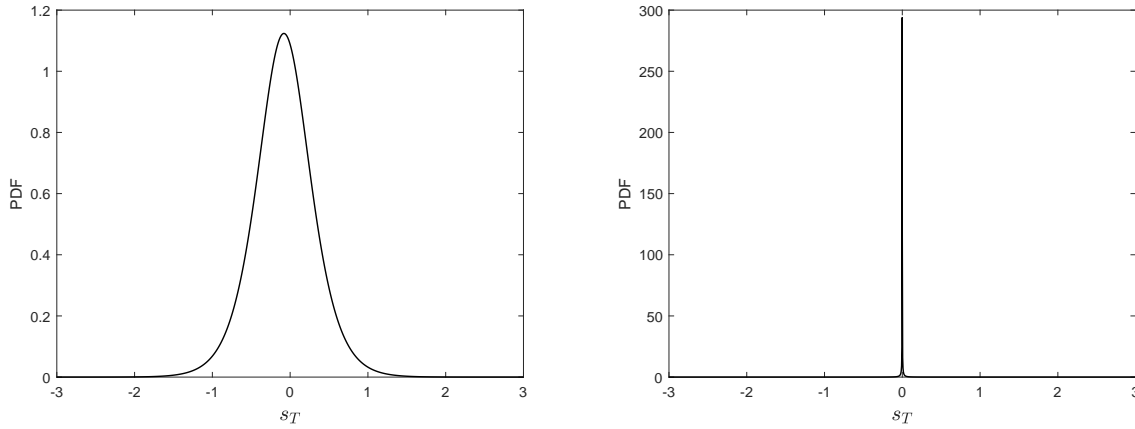
4.4 The rough Heston model

A more fashionable example is finally given by the rHeston model. We recall it in the following for readers' convenience.

Table 4: Relative errors over PV and CoN put options for *SINC* and *COS* at different values of N_F with the CGMY process. Stars (\star) mean that the price fully conforms with the benchmark (up to the number of digits of the benchmark itself), straight lines denote relative errors that are larger than 100%. [$Y = 1.5$, $T = 1$, $X_c = 33.0891$]

	K	PV put						benchmark	CoN put						benchmark
		N_F							N_F						
		16	32	48	64	96	128		16	32	48	64	96	128	
SINC	0.60	4e-02	5e-05	1e-09	*	*	*	0.1703012777	2e-05	*	*	*	*	*	0.3030356173
COS		1e-01	1e-02	6e-04	1e-05	9e-10	*		4e-02	6e-03	4e-04	2e-05	2e-09	*	
SINC	0.70	5e-02	9e-08	6e-10	*	*	*	0.2230381363	2e-05	*	*	*	*	*	0.3838662218
COS		1e-01	8e-03	3e-04	4e-06	6e-11	*		6e-02	9e-03	7e-04	2e-05	2e-09	*	
SINC	0.80	5e-02	3e-05	2e-09	*	*	*	0.2797474350	2e-05	*	*	*	*	*	0.4678295710
COS		7e-02	4e-03	7e-05	2e-06	5e-10	*		7e-02	1e-02	8e-04	2e-05	2e-09	*	
SINC	0.90	5e-02	4e-05	2e-09	*	*	*	0.3398136494	2e-05	*	*	*	*	*	0.5541526890
COS		4e-02	1e-03	1e-04	7e-06	8e-10	*		9e-02	1e-02	8e-04	2e-05	6e-10	*	
SINC	1.00	4e-02	4e-05	2e-09	*	*	*	0.4027464727	2e-05	*	*	*	*	*	0.6422747911
COS		2e-02	1e-03	2e-04	1e-05	8e-10	*		9e-02	1e-02	8e-04	2e-05	3e-10	*	
SINC	1.10	4e-02	4e-05	2e-09	*	*	*	0.4681498500	1e-05	*	*	*	*	*	0.7317810268
COS		6e-03	3e-03	3e-04	1e-05	6e-10	*		1e-01	1e-02	7e-04	1e-05	1e-09	*	
SINC	1.20	4e-02	3e-05	1e-09	*	*	*	0.5356998308	6e-06	*	*	*	*	*	0.8223594103
COS		7e-03	4e-03	4e-04	1e-05	3e-10	*		1e-01	1e-02	6e-04	6e-06	2e-09	*	
SINC	1.30	3e-02	2e-05	1e-09	*	*	*	0.6051284646	8e-07	*	*	*	*	*	0.9137720089
COS		2e-02	5e-03	4e-04	1e-05	3e-11	*		1e-01	1e-02	5e-04	1e-06	2e-09	*	
SINC	1.40	3e-02	1e-05	1e-09	*	*	*	0.6762118959	4e-06	*	*	*	*	*	1.0058351838
COS		3e-02	6e-03	4e-04	1e-05	2e-10	*		1e-01	1e-02	4e-04	4e-06	2e-09	*	

Figure 1: PDF of the asset log-price under CGMY process for $T = 1$ (lhs) and $T = 0.01$ (rhs). Parameters: $C = 1, G = 5, M = 5, Y = 0.5$.



The (generalized) rough Heston model from El Euch and Rosenbaum (2018) is described by the following equations:

$$ds_t = s_t \sqrt{V_t} \{ \rho dB_t + \sqrt{1 - \rho^2} dB_t^\perp \},$$

Table 5: Relative errors over PV and CoN put options for *SINC* and *COS* at different values of N_F with the CGMY process. Stars (\star) mean that the price fully conforms with the benchmark (up to the number of digits of the benchmark itself), straight lines denote relative errors that are larger than 100%. [$Y = 1.5$, $T = 0.01$, $X_c = 11.4582$]

	K	PV put							benchmark	CoN put						
		N_F								N_F						
		16	32	64	128	256	512		16	32	64	128	256	512	benchmark	
SINC	0.60	—	—	—	1e-01	*	*	0.0000620913	—	—	5e-03	1e-08	*	*	0.0006501357	
COS		—	—	—	—	1e-02	*		—	—	—	—	6e-03	1e-08		
SINC	0.70	—	—	—	5e-02	1e-07	*	0.0003572838	—	8e-01	4e-03	*	*	*	0.0044404620	
COS		—	—	—	6e-01	3e-03	*		—	—	—	8e-01	4e-03	*		
SINC	0.80	—	—	8e-01	1e-03	*	*	0.0021896005	8e-01	2e-01	1e-03	*	*	*	0.0320163483	
COS		—	—	—	6e-02	2e-04	*		—	—	8e-01	2e-01	1e-03	*		
SINC	0.90	—	8e-01	3e-02	2e-03	*	*	0.0124149741	4e-01	5e-02	2e-04	7e-10	*	*	0.1764020073	
COS		—	—	3e-01	2e-02	1e-04	*		—	9e-01	4e-01	5e-02	2e-04	7e-10		
SINC	1.00	6e-01	3e-01	5e-02	5e-04	1e-09	*	0.0475882889	2e-02	3e-03	4e-05	3e-11	*	*	0.5239991369	
COS		—	8e-01	2e-01	1e-02	4e-05	*		4e-02	3e-02	2e-02	3e-03	4e-05	3e-11		
SINC	1.10	3e-01	1e-01	1e-03	2e-04	*	*	0.1156677674	1e-01	1e-02	6e-05	1e-10	*	*	0.8929163078	
COS		8e-01	2e-01	2e-02	3e-03	1e-05	*		3e-01	2e-01	1e-01	1e-02	6e-05	1e-10		
SINC	1.20	2e-01	1e-02	1e-02	1e-04	*	*	0.2043804386	5e-02	7e-03	5e-05	1e-10	*	*	1.1281710458	
COS		3e-01	2e-02	3e-02	2e-03	7e-06	*		3e-01	2e-01	5e-02	7e-03	5e-05	1e-10		
SINC	1.30	1e-01	3e-02	2e-03	8e-05	*	*	0.3008048296	6e-03	5e-03	4e-05	3e-11	*	*	1.2743502846	
COS		9e-02	4e-02	3e-02	1e-03	6e-06	*		3e-01	2e-01	6e-03	5e-03	4e-05	3e-11		
SINC	1.40	6e-02	5e-02	7e-03	5e-05	2e-11	*	0.3995376021	4e-02	4e-03	2e-05	1e-10	*	*	1.3889715861	
COS		2e-03	6e-02	1e-02	1e-03	5e-06	*		3e-01	9e-02	4e-02	4e-03	2e-05	1e-10		

$$V_t = V_0 + \frac{\lambda}{\Gamma(H + \frac{1}{2})} \int_0^t \frac{\theta^0(s) - V_s}{(t-s)^{\frac{1}{2}-H}} ds + \frac{\nu}{\Gamma(H + \frac{1}{2})} \int_0^t \frac{\sqrt{V_s}}{(t-s)^{\frac{1}{2}-H}} dB_s,$$

where V_0 , λ , and ν are positive real numbers, $\rho \in [-1, 1]$. The deterministic function $\theta^0(t)$ is positive and satisfies few constraints specified in El Euch and Rosenbaum (2018). The coefficient $H \in (0, 1/2]$ is shown to govern the smoothness of the volatility, whose trajectories enjoy Hölder continuity $H - \epsilon$ for any $\epsilon > 0$. It is therefore clear that the choice $H < 1/2$ allows for a rough behavior of the volatility process and the case $H = 1/2$ amounts to the classical Heston model with time-dependent mean reversion level.

El Euch and Rosenbaum (2018) proved also that the product $\lambda\theta^0(\cdot)$ is directly inferred from the time-0 forward variance curve $\xi_0(t) = \mathbb{E}[V_t | \mathcal{F}_0] = \mathbb{E}[V_t]$, leading to the following specification of the model for $\lambda \rightarrow 0$:

$$dS_t = S_t \sqrt{V_t} \{ \rho dB_t + \sqrt{1 - \rho^2} dB_t^\perp \},$$

$$V_t = \xi_0(t) + \frac{\nu}{\Gamma(H + \frac{1}{2})} \int_0^t \frac{\sqrt{V_s}}{(t-s)^{\frac{1}{2}-H}} dB_s.$$

Table 6: Relative errors over PV and CoN put options for *SINC* and *COS* at different values of N_F with the CGMY process. Stars (\star) mean that the price fully conforms with the benchmark (up to the number of digits of the benchmark itself), straight lines denote relative errors that are larger than 100%. [$Y = 1.98$, $T = 1$, $X_c = 248.9047$]

	K	PV put						benchmark	CoN put						benchmark
		N_F							N_F						
		16	32	48	64	96	128		16	32	48	64	96	128	
SINC	0.60	1e-02	1e-05	6e-10	*	*	*	0.5429017201	5e-06	*	*	*	*	*	0.5429020811
COS		2e-02	3e-03	1e-04	2e-06	2e-10	*		1e-02	4e-03	9e-05	5e-06	3e-10	*	
SINC	0.70	1e-02	1e-05	4e-10	*	*	*	0.6333854028	5e-06	*	*	*	*	*	0.6333857942
COS		2e-02	3e-03	1e-04	3e-06	*	*		1e-02	4e-03	8e-05	5e-06	2e-10	*	
SINC	0.80	1e-02	1e-05	5e-10	*	*	*	0.7238690896	5e-06	*	*	*	*	*	0.7238695094
COS		2e-02	3e-03	1e-04	3e-06	1e-10	*		1e-02	4e-03	7e-05	5e-06	2e-10	*	
SINC	0.90	1e-02	1e-05	4e-10	*	*	*	0.8143527799	5e-06	*	*	*	*	*	0.8143532263
COS		1e-02	3e-03	1e-04	3e-06	1e-10	*		1e-02	4e-03	7e-05	5e-06	2e-10	*	
SINC	1.00	9e-03	1e-05	4e-10	*	*	*	0.9048364731	5e-06	*	*	*	*	*	0.9048369446
COS		1e-02	4e-03	1e-04	3e-06	*	*		1e-02	4e-03	6e-05	5e-06	2e-10	*	
SINC	1.10	9e-03	1e-05	4e-10	*	*	*	0.9953201687	5e-06	*	*	*	*	*	0.9953206642
COS		1e-02	4e-03	1e-04	3e-06	1e-10	*		1e-02	4e-03	5e-05	5e-06	2e-10	*	
SINC	1.20	8e-03	1e-05	3e-10	*	*	*	1.0858038665	5e-06	*	*	*	*	*	1.0858043849
COS		1e-02	4e-03	1e-04	3e-06	1e-10	*		9e-03	4e-03	5e-05	5e-06	2e-10	*	
SINC	1.30	8e-03	9e-06	4e-10	*	*	*	1.1762875661	5e-06	*	*	*	*	*	1.1762881065
COS		1e-02	4e-03	1e-04	3e-06	2e-10	*		9e-03	4e-03	4e-05	5e-06	2e-10	*	
SINC	1.40	8e-03	9e-06	3e-10	*	*	*	1.2667712674	5e-06	*	*	*	*	*	1.2667718289
COS		1e-02	4e-03	1e-04	3e-06	2e-10	*		9e-03	4e-03	4e-05	5e-06	2e-10	*	

This is extremely convenient for calibration purposes thanks to the reduced dimensionality of the problem. We will consequently work under this last specification throughout the rest of the paper, thus placing ourselves in the same setting of El Euch et al. (2019). Indeed our final point with the rHeston model will be to show that the SINC approach is a very efficient solution for calibration. This will be the content of the following section.

The forward variance curve is a state variable in the model and it also enters the CF of the asset log-price (see El Euch and Rosenbaum (2018) for further details):

$$\varphi(a, t) = \mathbb{E} \left[\exp \left\{ ia \log \left(\frac{S_t}{S_0} \right) \right\} \right] = \exp \left(\int_0^t D^\alpha h(a, t-s) \xi_0(s) ds \right),$$

where $\alpha = H + \frac{1}{2}$, $h(a, t)$ is the unique continuous solution of the fractional Riccati equation

$$D^\alpha h(a, t) = -\frac{1}{2}a(a+i) + iap\nu h(a, t) + \frac{\nu^2}{2}h^2(a, t), \quad I^{1-\alpha}h(a, 0) = 0, \quad (17)$$

and D^α , $I^{1-\alpha}$ denote the Riemann-Liouville fractional derivative and fractional integral of

Table 7: Relative errors over PV and CoN put options for *SINC* and *COS* at different values of N_F with the CGMY process. Stars (\star) mean that the price fully conforms with the benchmark (up to the number of digits of the benchmark itself), straight lines denote relative errors that are larger than 100%. [$Y = 1.98$, $T = 0.01$, $X_c = 24.9357$]

		PV put						benchmark	CoN put						benchmark
		N_F							N_F						
	K	16	32	48	64	96	128		16	32	48	64	96	128	
SINC	0.60	4e-02	5e-05	*	*	*	*	0.1359287091	2e-06	*	*	*	*	*	0.2916287066
COS		2e-01	2e-02	6e-04	1e-05	*	*		9e-03	1e-03	9e-05	2e-06	3e-10	*	
SINC	0.70	5e-02	2e-06	9e-10	*	*	*	0.1877507817	7e-06	*	*	*	*	*	0.3840967883
COS		2e-01	1e-02	4e-04	7e-06	6e-10	*		3e-02	4e-03	3e-04	7e-06	7e-11	*	
SINC	0.80	5e-02	3e-05	*	*	*	*	0.2453606494	1e-05	*	*	*	*	*	0.4816538267
COS		1e-01	8e-03	2e-04	2e-06	*	*		5e-02	8e-03	5e-04	1e-05	2e-10	*	
SINC	0.90	4e-02	4e-05	*	*	*	*	0.3079042304	1e-05	*	*	*	*	*	0.5828557330
COS		8e-02	4e-03	5e-05	1e-06	*	*		7e-02	1e-02	6e-04	1e-05	2e-10	*	
SINC	1.00	4e-02	3e-05	*	*	*	*	0.3746672106	1e-05	*	*	*	*	*	0.6866524319
COS		5e-02	1e-03	8e-05	3e-06	*	*		8e-02	1e-02	5e-04	1e-05	3e-11	*	
SINC	1.10	3e-02	3e-05	9e-11	*	*	*	0.4450537289	6e-06	*	*	*	*	*	0.7922765311
COS		3e-02	8e-04	2e-04	5e-06	1e-10	*		9e-02	1e-02	5e-04	7e-06	2e-10	*	
SINC	1.20	3e-02	2e-05	*	*	*	*	0.5185661093	3e-06	*	*	*	*	*	0.8991643649
COS		1e-02	2e-03	2e-04	5e-06	5e-11	*		1e-01	1e-02	4e-04	3e-06	3e-10	*	
SINC	1.30	2e-02	9e-06	2e-10	*	*	*	0.5947873571	2e-07	*	*	*	*	*	1.0069001160
COS		1e-04	4e-03	3e-04	5e-06	*	*		1e-01	1e-02	3e-04	1e-07	3e-10	*	
SINC	1.40	2e-02	1e-06	2e-10	*	*	*	0.6733666332	3e-06	*	*	*	*	*	1.1151760866
COS		1e-02	5e-03	3e-04	4e-06	*	*		1e-01	1e-02	2e-04	3e-06	3e-10	*	

order α and $1 - \alpha$, respectively ⁵.

Now, Equation (17) is a rough version of the Riccati ODE which emerges in the classical Heston model with zero mean reversion. Here, the standard derivative is replaced by a fractional one. However, such a small change has relevant implications. The rHeston Riccati equation has no explicit solution and needs to be solved using numerical methods which are not really plain. We are not discussing the general issue of an efficient computation of the CF, which topic has been largely debated in the last few years (from a standard appli-

⁵The Riemann-Liouville fractional derivative of a function f is defined as

$$D^\alpha f(t) = \frac{1}{\Gamma(1-\alpha)} \frac{d}{dt} \int_0^t (t-s)^{-\alpha} f(s) ds \quad \alpha \in [0, 1),$$

provided that it exists. Similarly the fractional integral, provided that it exists, is given by

$$I^\alpha f(t) = \frac{1}{\Gamma(\alpha)} \int_0^t (t-s)^{\alpha-1} f(s) ds \quad \alpha \in (0, 1].$$

Table 8: Relative errors over PV and CoN put options for *SINC* and COS at different values of N_F with the CGMY process. Stars (\star) mean that the price fully conforms with the benchmark (up to the number of digits of the benchmark itself), straight lines denote relative errors that are larger than 100%. [$Y = 0.5$, $T = 1$, $X_c = 18.3512$]

		PV put							CoN put						
		N_F							benchmark	N_F					
	K	16	32	64	128	256	512	16		32	64	128	256	512	
SINC	0.60	5e-01	7e-01	2e-02	3e-05	*	*	0.0083082000	5e-02	8e-04	8e-07	*	*	*	0.0453996882
COS		—	1e-01	1e-01	2e-03	2e-06	*		—	8e-01	5e-02	8e-04	8e-07	*	
SINC	0.70	—	2e-01	3e-03	9e-06	*	*	0.0189241836	4e-02	2e-03	2e-06	*	*	*	0.0984380619
COS		—	3e-01	4e-02	2e-04	8e-07	*		—	5e-01	4e-02	2e-03	2e-06	*	
SINC	0.80	8e-01	6e-03	4e-03	6e-06	*	*	0.0371703257	5e-02	1e-04	1e-06	2e-11	*	*	0.1819799859
COS		—	4e-01	5e-03	6e-04	6e-07	*		—	6e-01	3e-01	5e-02	1e-04	1e-06	2e-11
SINC	0.90	5e-01	6e-02	1e-04	5e-06	*	*	0.0648967583	3e-02	1e-03	3e-07	6e-11	*	*	0.2956669642
COS		—	3e-01	2e-02	4e-05	5e-07	*		—	2e-01	1e-01	3e-02	1e-03	3e-07	6e-11
SINC	1.00	4e-01	6e-02	2e-03	3e-06	*	*	0.1029669064	4e-03	2e-04	8e-07	3e-10	*	*	0.4323807669
COS		9e-01	2e-01	2e-02	3e-04	3e-07	*		—	3e-02	2e-02	4e-03	2e-04	8e-07	3e-10
SINC	1.10	3e-01	5e-02	1e-03	4e-07	*	*	0.1511107358	1e-02	5e-04	1e-06	*	*	*	0.5813874463
COS		6e-01	1e-01	1e-02	1e-04	6e-08	*		—	9e-02	5e-02	1e-02	5e-04	1e-06	*
SINC	1.20	2e-01	3e-02	9e-05	2e-06	*	*	0.2082023058	2e-02	5e-04	8e-07	3e-11	*	*	0.7328465863
COS		4e-01	9e-02	4e-03	8e-05	1e-07	*		—	2e-01	8e-02	2e-02	5e-04	8e-07	3e-11
SINC	1.30	2e-01	2e-02	5e-04	5e-07	*	*	0.2727258052	2e-02	5e-05	5e-07	*	*	*	0.8803504028
COS		3e-01	4e-02	2e-03	1e-04	1e-07	*		—	2e-01	1e-01	2e-02	5e-05	5e-07	*
SINC	1.40	1e-01	4e-03	6e-04	1e-06	4e-11	*	0.3431572893	1e-02	3e-04	8e-07	3e-11	*	*	1.0208938948
COS		2e-01	1e-02	4e-03	7e-05	4e-08	*		—	2e-01	1e-01	1e-02	3e-04	8e-07	3e-11

cation of the Adams scheme of Diethelm et al. (2004) to more problem-specific techniques like the rational approximation of Gatheral and Radoicic (2019) and the hybrid method of Callegaro et al. (2020)). We simply claim that, given any approximation to the CF, the *SINC* is a very effective method to perform pricing and calibration. We will therefore stick with the rational approximation to the CF of Gatheral and Radoicic (2019) to compute the CF, and discuss our results within that setting. The interested reader is referred to the original paper for a complete discussion about the approximation; in particular, Equations (4.1) and (4.12)-(4.17) in Gatheral and Radoicic (2019) will do most of the job.

We use the following parameters for the experiments that follow

$$S_0 = 1 \quad r = 0 \quad q = 0 \quad T = \{0.01, 1\} \quad H = 0.05 \quad \nu = 0.4 \quad \rho = -0.65,$$

and assume the forward variance curve is flat at $\xi_0(\cdot) = 0.0256$.

Let us start with the typical example where expiration is in 1 year, i.e. $T = 1$. As we

Table 9: Relative errors over PV and CoN put options for *SINC* and COS at different values of N_F with the CGMY process. Stars (★) mean that the price fully conforms with the benchmark (up to the number of digits of the benchmark itself), straight lines denote relative errors that are larger than 100%. [$Y = 0.5$, $T = 0.01$, $X_c = 12.0723$]

		PV put							CoN put						
		N_F						benchmark	N_F						benchmark
	K	256	512	1024	2048	4096	8192		256	512	1024	2048	4096	8192	
SINC	0.60	—	—	—	—	8e-01	5e-01	0.0000223408	—	—	8e-01	2e-01	8e-02	3e-03	0.0001785593
COS		—	—	6e-01	1e-01	2e-02	3e-03		—	—	—	—	8e-01	2e-01	
SINC	0.70	—	—	—	3e-01	7e-01	2e-01	0.0000799072	—	—	8e-02	2e-01	4e-02	5e-03	0.0006873067
COS		—	—	9e-02	4e-02	1e-02	3e-04		—	—	—	—	8e-02	2e-01	
SINC	0.80	—	6e-01	—	7e-01	2e-01	1e-02	0.0002674771	3e-01	8e-01	3e-01	7e-02	4e-03	4e-03	0.0025728961
COS		—	6e-01	2e-01	8e-03	2e-03	6e-04		—	—	3e-01	8e-01	3e-01	7e-02	
SINC	0.90	—	2e-01	6e-01	2e-01	6e-02	7e-03	0.0009262546	2e-01	5e-01	2e-01	4e-02	5e-03	2e-03	0.0110260134
COS		2e-01	2e-01	1e-01	5e-03	1e-03	3e-04		—	—	2e-01	5e-01	2e-01	4e-02	
SINC	1.00	1e-01	8e-02	4e-02	2e-02	6e-03	2e-03	0.0060510208	1e-01	9e-02	8e-02	6e-02	3e-02	1e-02	0.4459496554
COS		—	5e-01	2e-01	6e-02	2e-02	5e-03		1e-01	1e-01	1e-01	9e-02	8e-02	6e-02	
SINC	1.10	4e-02	2e-02	6e-03	2e-03	5e-04	2e-05	0.1004887993	2e-02	6e-03	2e-03	5e-04	2e-05	3e-05	1.0832677912
COS		1e-02	1e-03	9e-05	3e-05	2e-05	5e-06		8e-02	4e-02	2e-02	6e-03	2e-03	5e-04	
SINC	1.20	2e-02	5e-03	6e-04	1e-03	3e-04	2e-05	0.1995452121	5e-03	6e-04	1e-03	3e-04	2e-05	2e-05	1.1929282653
COS		4e-03	1e-03	3e-04	7e-05	5e-06	1e-06		4e-02	2e-02	5e-03	6e-04	1e-03	3e-04	
SINC	1.30	2e-03	6e-03	2e-03	7e-05	3e-04	6e-05	0.2991115246	6e-03	2e-03	7e-05	3e-04	6e-05	1e-05	1.2958046554
COS		3e-03	9e-04	5e-05	2e-05	7e-06	2e-07		2e-02	2e-03	6e-03	2e-03	7e-05	3e-04	
SINC	1.40	1e-02	3e-03	1e-04	6e-04	2e-04	4e-05	0.3988490890	3e-03	1e-04	6e-04	2e-04	4e-05	4e-06	1.3969698655
COS		3e-03	2e-04	8e-05	2e-05	4e-07	2e-07		3e-03	1e-02	3e-03	1e-04	6e-04	2e-04	

always did throughout this section, we report convergence results for PV and digital put options (AoN in this case) in Table 10. We have often observed a gap in the performances of the *SINC* and the COS method when dealing with PV options and we have learnt that the gap gets larger when moving to their digital components. This time it is not different. Therefore, it would be the case that we try to understand where such a behavior comes from and we refer to the following Figure (2) in doing so ⁶.

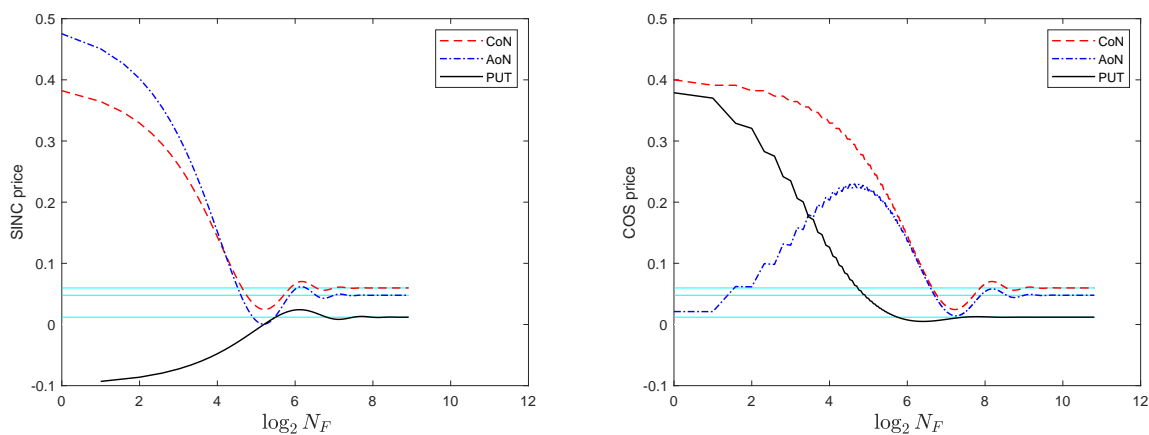
The idea behind these charts is that we take our benchmarks as a reference, compute prices with the two methods by increasing N_F of one unit per time and stop when we have reached satisfactory accuracy (say 8 digits) on both CoN and AoN puts. Not surprisingly, then, the *SINC* is shown to meet the target for much lower N_F , and the oscillations on the digital options last longer on the rhs than the lhs of the figure. Also, digital options are less stable than PV puts, for both the methods, but the composition of CoN and AoN

⁶We only focus on options which are struck at $K = 0.80$ but stress that the pattern does not depend on the moneyness (as one can guess from Table 10).

Table 10: Relative errors over PV and AoN put options for *SINC* and COS at different values of N_F in the rough Heston model. Stars (\star) mean that the price fully conforms with the benchmark (up to the number of digits of the benchmark itself), straight lines denote relative errors that are larger than 100%. [$T = 1$, $X_c = 18.9469$]

	K	PV put						benchmark	dig put						benchmark
		N_F							N_F						
		256	512	768	1024	1536	2048		256	512	768	1024	1536	2048	
SINC	0.60	2e-02	6e-03	2e-05	2e-06	*	*	0.003190745	4e-03	2e-06	*	*	*	*	0.0105749538
COS		8e-02	6e-03	3e-04	3e-05	1e-06	*		2e-01	2e-02	1e-02	2e-03	2e-05	9e-07	
SINC	0.70	4e-02	3e-03	6e-05	3e-07	*	*	0.006322036	2e-03	2e-07	*	*	*	*	0.0226378550
COS		6e-02	4e-03	1e-05	6e-05	3e-07	*		9e-02	3e-02	1e-02	1e-03	4e-05	3e-08	
SINC	0.80	1e-02	1e-03	3e-05	2e-07	*	*	0.011948775	2e-03	5e-07	*	*	*	*	0.0477997904
COS		5e-02	4e-03	4e-04	1e-05	9e-07	*		1e-01	3e-03	5e-03	1e-03	2e-05	4e-07	
SINC	0.90	3e-02	1e-03	2e-05	4e-07	*	*	0.022432028	1e-03	5e-07	*	*	*	*	0.1081020775
COS		4e-02	2e-03	3e-04	3e-05	6e-07	*		2e-01	3e-02	6e-03	1e-03	2e-05	4e-07	
SINC	1.00	2e-03	4e-04	8e-06	1e-07	*	*	0.045518977	7e-04	3e-07	*	*	*	*	0.3222614106
COS		2e-02	2e-03	4e-04	3e-05	9e-07	*		1e-01	2e-02	2e-04	6e-04	7e-06	3e-07	
SINC	1.10	3e-03	7e-05	5e-06	9e-08	*	*	0.108597244	3e-04	1e-08	*	*	*	*	0.8378414609
COS		1e-03	1e-03	1e-04	6e-06	3e-07	2e-10		6e-02	3e-03	1e-03	3e-04	6e-06	4e-09	
SINC	1.20	3e-03	8e-05	1e-06	3e-10	*	*	0.202190574	3e-05	4e-08	*	*	*	*	0.9673515242
COS		5e-03	5e-04	7e-05	9e-06	2e-07	*		3e-02	4e-03	5e-04	5e-05	4e-07	4e-08	
SINC	1.30	3e-03	8e-05	2e-06	3e-08	*	*	0.300785493	8e-05	3e-08	*	*	*	*	0.9898679762
COS		4e-03	2e-04	3e-05	3e-06	5e-08	*		1e-02	4e-03	4e-04	1e-04	2e-06	4e-08	
SINC	1.40	2e-03	7e-05	2e-06	3e-08	*	*	0.400341035	7e-05	2e-08	*	*	*	*	0.9960163357
COS		1e-03	8e-05	1e-05	2e-06	3e-08	*		2e-02	3e-03	6e-04	9e-05	2e-06	3e-08	

Figure 2: Convergence of the *SINC* (lhs) and the COS (rhs) method. Red (dashed), blue (dot-dashed), and black (bold) lines are the CoN, AoN, and put options, respectively. Light blue horizontal lines denote the benchmarks. $T = 1$ and $K = 0.80$.



options introduces cancellations that are beneficial to the COS much more than they are to the *SINC*. This, in fact, explains PV put prices within the COS to finally catch up the *SINC*.

Moreover, we also consider the challenging case where $T = 0.01$. If this seems too short, it is still something one may encounter during the calibration process, and it goes in the direction of pricing the weekly options. We consequently produce Table 11 and accompany it by Figure (3) (where we study the case $K = 0.80$ in more details).

Table 11: Relative errors over PV and AoN put options for *SINC* and COS at different values of N_F in the rough Heston model. Stars (\star) mean that the price fully conforms with the benchmark (up to the number of digits of the benchmark itself), straight lines denote relative errors that are larger than 100%. [$T = 0.01$, $X_c = 2.7074$]

		PV put							AoN put						
		N_F							benchmark	N_F					
	K	256	512	768	1024	1536	2048	benchmark	256	512	768	1024	1536	2048	benchmark
SINC	0.60	—	—	—	—	6e-01	*	0.0000000002	—	—	1e-02	*	*	*	0.0000000046
COS		—	—	—	—	—	*		—	—	—	—	—	—	
SINC	0.70	—	—	—	—	*	*	0.0000000086	—	3e-01	1e-04	*	*	*	0.0000002286
COS		—	—	—	—	1e-01	*		—	—	—	—	—	2e-01	
SINC	0.80	—	—	8e-01	4e-03	*	*	0.0000005625	—	8e-04	7e-06	*	*	*	0.0000188150
COS		—	—	5e-01	5e-02	2e-03	*		—	—	—	—	9e-02	7e-04	
SINC	0.90	7e-01	2e-01	2e-03	6e-04	*	*	0.0000422546	5e-02	1e-04	2e-07	*	*	*	0.0016079673
COS		4e-01	1e-01	1e-02	8e-04	1e-04	*		—	2e-01	1e-01	4e-02	7e-04	1e-04	
SINC	1.00	4e-03	2e-03	1e-05	5e-06	*	*	0.0050767335	1e-03	4e-06	7e-09	*	*	*	0.3546252030
COS		4e-02	3e-03	1e-03	2e-04	6e-06	3e-07		2e-01	4e-02	2e-03	1e-03	1e-04	4e-06	
SINC	1.10	6e-05	1e-04	5e-07	3e-07	1e-09	*	0.1000001857	1e-04	3e-07	5e-10	*	*	*	0.9999913370
COS		5e-04	7e-05	8e-06	4e-07	7e-08	1e-09		8e-03	8e-05	3e-04	1e-04	1e-06	3e-07	
SINC	1.20	6e-04	9e-06	3e-06	1e-07	*	*	0.2000000119	1e-05	1e-07	1e-10	*	*	*	0.9999996919
COS		2e-04	2e-05	4e-07	5e-07	7e-09	2e-10		2e-03	8e-04	2e-04	1e-05	3e-06	2e-07	
SINC	1.30	4e-04	9e-06	2e-06	9e-08	*	*	0.3000000020	8e-06	1e-07	1e-10	*	*	*	0.9999999577
COS		4e-05	7e-06	1e-06	3e-07	5e-09	4e-10		4e-03	5e-04	4e-05	1e-05	2e-06	1e-07	
SINC	1.40	3e-04	8e-06	2e-06	7e-08	*	*	0.4000000005	8e-06	7e-08	6e-11	*	*	*	0.9999999902
COS		6e-05	4e-06	3e-07	2e-07	4e-09	3e-10		2e-03	4e-04	2e-04	1e-05	2e-06	1e-07	

One difference with respect to the case $T = 1$ that one can immediately spot is that digital options (and PV, as a consequence) tend to oscillate more with very short maturities. For example, when $N_F = 256$ neither *SINC* nor COS provide meaningful values when the option is out-of-the-money. Again, this is a consequence of Fact 3 that we have listed. Figure (4) reports the PDFs for visual aid.

While this concludes our analysis for the convergence of the *SINC* approach, one last comment is in order about Fact 2. We have seen that convenient selection of the bounds for the integration range guarantees (more or less) fast convergence to the "true" option

Figure 3: Convergence of the *SINC* (lhs) and the *COS* (rhs) method. Red (dashed), blue (dot-dashed), and black (bold) lines are the CoN, AoN, and put options, respectively. Light blue horizontal lines denote the benchmarks. $T = 0.01$ and $K = 0.80$.

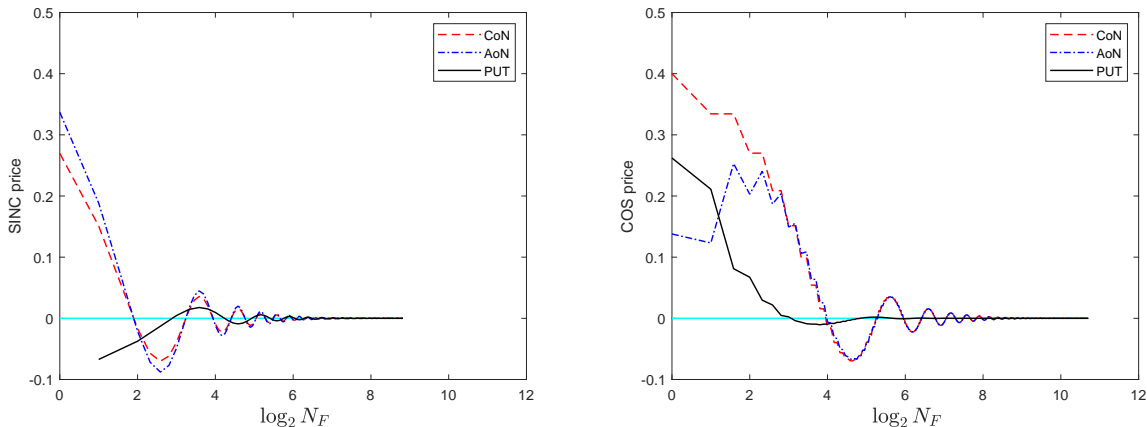
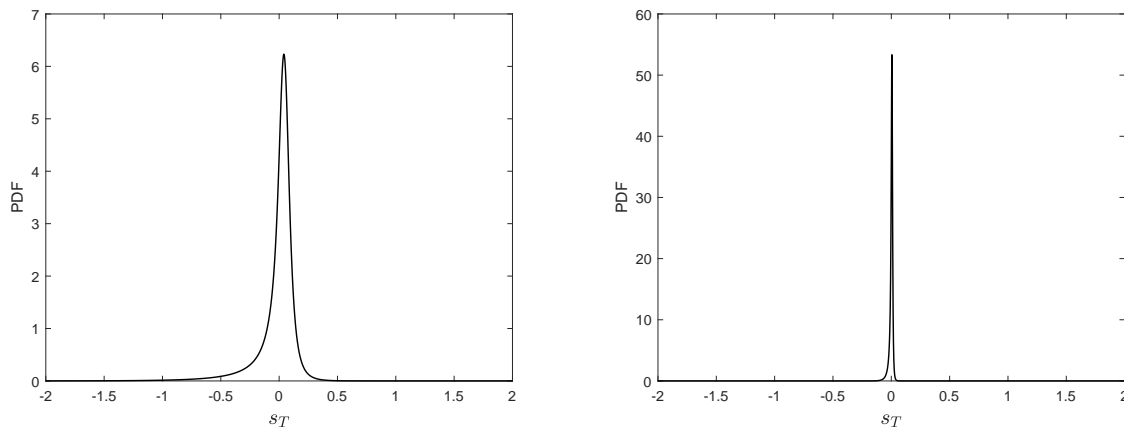


Figure 4: PDF of the asset log-price under the rHeston model for $T = 1$ (lhs) and $T = 0.01$ (rhs). Parameters: $H = 0.05, \nu = 0.40, \rho = -0.65$.



price, and this is a strong empirical indication as not to worry about the contribution of error terms ϵ_2 and ϵ_3 (whose numerical characterization would critically depend on the particular model at hand). This very comforting practical regularity that we observe for all the models we have considered is sometimes violated by the rHeston model: when the expiration is long enough it is in fact true that the agreement between high precision *SINC* and *COS* candidates is only ensured to reach 8/9 decimal digits. One way to fix this issue is to multiply the computed X_c by some factor, which fact suffices to impute the cause of

such a little lack of accuracy to ϵ_3 (recall that the magnitude of ϵ_2 only depends on N). Then, by the definition of ϵ_3 we know that it associates with the replacement of the CF of the truncated density with the CF of the complete one, thus suggesting some little issue with the numerical approximation of the solution to the fractional Riccati equation which should be investigated more carefully.

5 Accuracy and Efficiency of FFT-*SINC*

If our earlier comparison with the COS method depicts the *SINC* as a very accurate solution for Fourier pricing and (often times) it shows improved convergence with respect to the cosine expansion, one may be obviously interested in testing the FFT version of subsection 2.1 against standard techniques of the same type. Availability of an FFT method is crucial for large scale problems such as calibration – where several strikes have to be computed simultaneously for any given maturity – and this is the main reason why Carr-Madan traditional technique or (a naive discretization of) Lewis formula are often preferred to the COS, for such practical purposes: at the end of the day, some lack of accuracy due to interpolation error may be an acceptable price to pay for the $N \log(N)$ computational complexity of the FFT algorithm. We therefore challenge FFT-*SINC* against such methodologies in the attempt to show that it requires much lower N_F to reach satisfactory accuracy on the implied volatilities. In case this is achieved, then we may well regard FFT-*SINC* as a benchmark method in terms of efficiency as well.

Before we proceed in this direction we slightly elaborate on Lewis formula so as to clarify what we mean by a naive discretization. The reader will recognize Equation (18) as the price of a PV call option under Lewis (2000):

$$C(S, K, T) = S - \frac{\sqrt{SK}}{\pi} \int_0^{+\infty} \Re \left[e^{-iuk} \phi_T \left(u - \frac{i}{2} \right) \right] \frac{du}{u^2 + \frac{1}{4}}. \quad (18)$$

We are assuming zero interest rate and dividend yield here and denote $\phi_T(\cdot)$ the CF of the asset log-price. So, once a proper bound u_{\max} has been defined for the integral above, and

according to the strike grid

$$K_v = e^{k_v}, \quad k_v = -b + \gamma v \quad v = 0, \dots, N-1 \quad b = \frac{N\gamma}{2} \quad \gamma = \frac{2\pi}{N\eta} \quad \eta = \frac{u_{\max}}{N-1}$$

one can discretize Equation (18) as

$$C(S, K_v, T) \approx S - \frac{\sqrt{SK_v}}{\pi} \sum_{j=0}^{N-1} {}' \Re \left[e^{iu_j b} e^{-i\frac{2\pi}{N} j v} \phi_T \left(u_j - \frac{i}{2} \right) \right] \frac{\eta}{u_j^2 + \frac{1}{4}}, \quad u_j = \eta j \quad (19)$$

where $\sum {}'$ indicates that the first term in the sum is multiplied by $\frac{1}{2}$. Simpson weights may be used as well (this is the suggestion from Carr and Madan (1999), for example), but we do not see any improvement when this is done.

This very much resembles the approach by Carr and Madan (1999) in many respects and both are easily generalized to the frFFT if needed. The paper by Chourdakis (2005) provides the details for the implementation.

For the purposes of comparison, we now get back to the rough Heston model and price the same volatility surfaces as in El Euch et al. (2019). We maintain the forward variance form that we have reported in the previous section and make the forward variance curve flat for simplicity⁷. We use suitable parameters in pricing, invert for the implied volatility and report the lowest N_F that we need to make the average absolute error on the volatilities of the order 10^{-6} , over each smile. Then, the idea is that this will establish a hierarchy of the different methods.

As this will not appear in our study, benchmark prices are computed via high-precision COS; implied volatilities are calculated on those benchmarks and absolute differences referenced to them.

⁷In a concrete situation the standard strategy is to estimate the forward variance curve as a difference on the variance swap curve. The fair value of a variance swap is computed using the methodologies explained in Fukasawa (2012) and an iteration procedure is subsequently performed to match model and market at-the-money volatilities through shifting and scaling.

We have already noticed that the *SINC* approach requires a suitable truncation range for the PDF of the asset log-price to be calculated: we do so by the cutting procedure that we have explained and repeat the same exercise for every maturity in the volatility surface. This has a precise meaning within the *SINC* but it still may be (indirectly) linked to the choice of the upper limit of integration u_{\max} with Carr-Madan method and Lewis formula. We focus on the latter, here.

The periodicity of the sum (19) approximating the Lewis integral may in fact be linked to the choice of X_c for the *SINC* and exploited to choose the step size in the discretization grid η . However, since Lewis formula does not leverage the bounded support of the PDF as the *SINC* does, one should allow for an extra degree of freedom and accept the following definition

$$\eta = \frac{1}{2X_c\beta}$$

where β is to be optimally chosen so as to minimize the average distance over the surface between Lewis price and the benchmark. We stress that the choice for β depends on N_F and is to be repeated each time this is changed.

The exact same procedure holds true for Carr-Madan method but in general the optimal β 's will be different. Moreover, it is important to stress that the dumping parameter is also to be chosen for Carr-Madan. As a precise rule to fix it does not exist, we proceed by testing several values. The best performance we experience corresponds to the case $\alpha_{CM} = 0.4$.

The relation between N_F and u_{\max} (and α_{CM}) is not clearly understood in Lewis and Carr-Madan method, and no theoretical or heuristic argument is available to properly select the upper limit of integration, making it difficult to blindly trust those approaches. In this regard, having a straightforward interpretation for X_c in the *SINC* and a direct link with the option price approximation error should also be very much appreciated.

Coming to our numerical experiments, we have two volatility surfaces to be priced. The

first one is for the S&P500 as of August 14, 2013 and it consists of 19 expirations from a couple of days to about 2.5 years, for a total 1291 strike-expiration pairs. Calibrated parameters in El Euch et al. (2019) are given as:

$$H = 0.1216 \quad \nu = 0.2910 \quad \rho = -0.6714.$$

With these numbers we compute put option prices for the entire surface based on all of FFT methods above. We also advocate the frFFT versions for a complete overview of the results, that we quote in Table 12. We report the lowest N_F to reach the required accuracy per smile described in the previous paragraph.

The computed X_c vector for the *SINC* is available on GitHub⁸, and the β 's that connect them to the upper limit of integration u_{\max} in Lewis (2000) and Carr and Madan (1999) methods are also reported in Table 12.

Table 12: N_F values and β 's for average absolute errors on the implied volatilities to be at most 10^{-6} over each smile. *SINC*, Lewis and Carr-Madan methods are investigated in both the FFT and frFFT versions. Fractional parameter ϵ is chosen $\epsilon = 0.15$ for *SINC*, $\epsilon = 0.02$ for the others. [S&P500 index as of August 14, 2013 – assumption: forward variance curve flat at 0.0320]

	FFT			frFFT		
	SINC	Lewis	Carr-Madan	SINC	Lewis	Carr-Madan
N_F	8192	65536 \blacklozenge	\bullet	512	4096	16384
β		1.600	4.000		2.200	5.500

One immediately observes that FFT-*SINC* meets the target with relatively small N_F , and it is actually true that more precise volatilities can be easily calculated by just increasing it. On the other hand, Lewis formula and Carr-Madan method experience difficulties which are unknown to the *SINC*. Specifically, a naive discretization of Lewis integral fails to guarantee the desired accuracy on the volatilities for very short maturities (as the black diamond indicates) and Carr-Madan method does not go further than an average error of

⁸<https://github.com/fabioBaschetti/SINC-method>. This also contains the surfaces that we use and all the codes one needs to reproduce our results.

the order 10^{-5} , even at high N_F (this is seen in a bullet point in the table). Such issues are eventually solved resorting to the fractional FFT. Lewis formula now requires $N_F = 4096$ evaluations of the CF for each smile and Carr-Madan method also reaches the target. In any case the *SINC* still proves to be largely superior, with $N_F = 512$ evaluations only. The fractional parameter (ϵ) restricting the domain of the conjugate variable is made to be as small as one can, compatibly with the strike grid from the surface. The precise meaning of ϵ is more directly understood in Section G of the Appendix.

Similar patterns are found when we move to May 19, 2017. This second surface counts 3352 strike-expiration pairs, which are distributed over 35 maturities to cover basically the same period as before. We now use the parameters from Section 4.4

$$H = 0.0500 \quad \nu = 0.4000 \quad \rho = -0.6500$$

and also conserve a flat forward variance curve (at $\xi_0(t) = 0.0256$). While Table 13 shows larger values of N_F for all methods, thereby spotting a more complicated volatility surface, the relations between *SINC* and its competitors are unchanged. This corroborates our claims about the superior performance of the *SINC*.

Table 13: N_F values and β 's for average absolute errors on the implied volatilities to be at most 10^{-6} over each smile. *SINC*, Lewis and Carr-Madan methods are investigated in both the FFT and frFFT versions. Fractional parameter ϵ is chosen $\epsilon = 0.15$ for *SINC*, $\epsilon = 0.02$ for the others. [S&P500 index as of May 19, 2017 – assumption: forward variance curve flat at 0.0256]

	FFT			frFFT		
	SINC	Lewis	Carr-Madan	SINC	Lewis	Carr-Madan
N_F	16384	65536 ♦	•	2048	8192	16384
β		1.000	2.500		1.170	3.168

6 Conclusions

The paper investigates the *SINC* approach when pricing PV options. *SINC* is shown to be superior to well-known benchmark methodologies. At variance with COS, it allows for an immediate extension to the FFT form. This is essential in any calibration exercise. Prompted by our results, we claim that *SINC* is a promising approach, regarding both the precision it achieves and its numerical efficiency. The numbers we produce in Sections 4 and 5 leave little space for different interpretations, they cover enough models to support the claim that the method is flexible enough to deal with jump-diffusion as well as rough Heston models, with the obvious alert (as it is for all Fourier-based techniques) that it can only be applied when the CF of the asset log-price is known either in analytic or semi-analytic form.

The idea behind *SINC* is that one first writes put options as a linear combination of digital Asset-or-Nothing and Cash-or-Nothing options. The expectation defining their values is a convolution between the density of the asset log-return and the payoff function. Then, the convolution theorem for Fourier transforms guarantees that each price can be expressed as the integral over a shifted CF. By approximating the CF of the true density with the CF of a truncated PDF, one can fully exploit the potential of the Shannon Sampling Theorem. It allows to represent the CF at any point by means of a discrete set of frequencies and express it as a Fourier-sinc expansion. The option price expressed in this form is the Modified Hilber transform of the sinc function that can be computed in close form yielding simple and compact formulas for digital and PV put option prices. Moreover, these formulas lend themselves to fast computation by means of FFT. The paper provides a rigorous proof of the convergence of the SINC formula to the correct option price when the support grows and the number of Fourier frequencies increases. It also investigates several technical prescriptions, such as the computation of truncation bounds by means of a cutting procedure based on the CDF. Conversely, if one wants to follow Fang and Oosterlee (2009) and their cumulants-based rule, we also provide a novel technique to compute them from the CF. The paper also addresses the issue of the sensitivity of the option prices to the number N_F of frequencies sampled in the Fourier-space. Through an extensive pricing exercise, it assesses the superior

performance of the *SINC* approach with respect to the competitor COS methodology. As far as the FFT specification is concerned, the paper challenges *SINC* against the FFT specification of the Lewis formula and the Carr-Madan approach. In both cases, *SINC* proves to be accurate and robust to option's specification.

References

- Bacry, E., S. Delattre, M. Hoffmann, and J.-F. Muzy (2013). Modelling microstructure noise with mutually exciting point processes. *Quantitative Finance* 13(1), 65–77.
- Bacry, E., T. Jaisson, and J.-F. Muzy (2016). Estimation of slowly decreasing Hawkes kernels: Application to high-frequency order book dynamics. *Quantitative Finance* 16(8), 1179–1201.
- Bakshi, G. S. and Z. Chen (1997). An alternative valuation model for contingent claims. *Journal of Financial Economics* 44(1), 123–165.
- Bates, D. S. (1996). Jumps and stochastic volatility: Exchange rate processes implicit in deutsche mark options. *The Review of Financial Studies* 9(1), 69–107.
- Bayer, C., C. Ben Hammouda, and R. Tempone (2020). Hierarchical adaptive sparse grids and quasi-Monte Carlo for option pricing under the rough bergomi model. *Quantitative Finance* 20(9), 1457–1473.
- Bayer, C., P. Friz, and J. Gatheral (2016). Pricing under rough volatility. *Quantitative Finance* 16(6), 887–904.
- Bennedsen, M., A. Lunde, and M. S. Pakkanen (2016). Decoupling the short-and long-term behavior of stochastic volatility. *ArXiv preprint arXiv:1610.00332*.
- Bennedsen, M., A. Lunde, and M. S. Pakkanen (2017). Hybrid scheme for Brownian semistationary processes. *Finance and Stochastics* 21(4), 931–965.
- Callegaro, G., M. Grasselli, and G. Pages (2021). Fast hybrid schemes for fractional Riccati equations (rough is not so tough). *Mathematics of Operations Research* 46(1) 221-254 .
- Carr, P. and D. Madan (1999). Option valuation using the fast Fourier transform. *Journal of Computational Finance* 2(4), 61–73.
- Carr, P., H. Geman, D. B. Madan, and M. Yor (2002). The fine structure of asset returns: An empirical investigation. *The Journal of Business* 75(2), 305–332.

- Chen, R.-R. and L. Scott (1992). Pricing interest rate options in a two-factor Cox–Ingersoll–Ross model of the term structure. *The Review of Financial Studies* 5(4), 613–636.
- Cherubini, U., G. Della Lunga, S. Mulinacci, and P. Rossi (2009). *Fourier Transform Methods in Finance*. John Wiley & Sons Inc.
- Chourdakis, K. (2005). Option pricing using the fractional FFT. *Journal of Computational Finance* 8(2), 1–18.
- Diethelm, K., N. J. Ford, and A. D. Freed (2004). Detailed error analysis for a fractional Adams method. *Numerical algorithms* 36(1), 31–52.
- Duffie, D., J. Pan, and K. Singleton (2000). Transform analysis and asset pricing for affine jump-diffusions. *Econometrica* 68(6), 1343–1376.
- El Euch, O., J. Gatheral, and M. Rosenbaum (2019). Roughening Heston. *Risk*, 84–89.
- El Euch, O. and M. Rosenbaum (2018, 12). Perfect hedging in rough Heston models. *The Annals of Applied Probability* 28(6), 3813–3856.
- El Euch, O. and M. Rosenbaum (2019). The characteristic function of rough Heston models. *Mathematical Finance* 29(1), 3–38.
- Fang, F. and C. W. Oosterlee (2009). A novel pricing method for european options based on Fourier-cosine series expansions. *SIAM Journal on Scientific Computing* 31(2), 826–848.
- Fukasawa, M. (2011). Asymptotic analysis for stochastic volatility: martingale expansion. *Finance and Stochastics* 15(4), 635–654.
- Fukasawa, M. (2012). The normalizing transformation of the implied volatility smile. *Mathematical Finance* 22(4), 753–762.
- Gatheral, J., T. Jaisson, and M. Rosenbaum (2018). Volatility is rough. *Quantitative Finance* 18(6), 933–949.
- Gatheral, J. and R. Radoicic (2019). Rational approximation of the rough Heston solution. *International Journal of Theoretical and Applied Finance* 22(3), 1950010.

- Hardiman, S. J., N. Bercot, and J.-P. Bouchaud (2013). Critical reflexivity in financial markets: a Hawkes process analysis. *The European Physical Journal B* 86(10), 442.
- Hawkes, A. G. (1971a). Point spectra of some mutually exciting point processes. *Journal of the Royal Statistical Society: Series B (Methodological)* 33(3), 438–443.
- Hawkes, A. G. (1971b). Spectra of some self-exciting and mutually exciting point processes. *Biometrika* 58(1), 83–90.
- Heston, S. L. (1993). A closed-form solution for options with stochastic volatility with applications to bond and currency options. *The Review of Financial Studies* 6(2), 327–343.
- Jaisson, T., M. Rosenbaum, et al. (2015). Limit theorems for nearly unstable Hawkes processes. *The Annals of Applied Probability* 25(2), 600–631.
- Jaisson, T., M. Rosenbaum, et al. (2016). Rough fractional diffusions as scaling limits of nearly unstable heavy tailed Hawkes processes. *The Annals of Applied Probability* 26(5), 2860–2882.
- Lewis, A. L. (2000). *Option Valuation Under Stochastic Volatility with Mathematica Code*. Finance Press: Newport Beach.
- Lewis, A. L. (2001). A simple option formula for general jump-diffusion and other exponential Lévy processes. *SSRN working paper*, <http://ssrn.com/abstract=282110>.
- Livieri, G., S. Mouti, A. Pallavicini, and M. Rosenbaum (2018). Rough volatility: Evidence from option prices. *IISE transactions* 50(9), 767–776.
- McCrickerd, R. and M. S. Pakkanen (2018). Turbocharging Monte Carlo pricing for the rough Bergomi model. *Quantitative Finance* 18(11), 1877–1886.
- Scott, L. O. (1997). Pricing stock options in a jump-diffusion model with stochastic volatility and interest rates: Applications of Fourier inversion methods. *Mathematical Finance* 7(4), 413–426.

Shannon, C. E. (1949). Communication in the presence of noise. *Proceedings of the IRE* 37(1), 10-21.

Appendix

A Inverse Fourier Transform of the θ Function

Let us look at the distribution δ^- and let us recall the definition

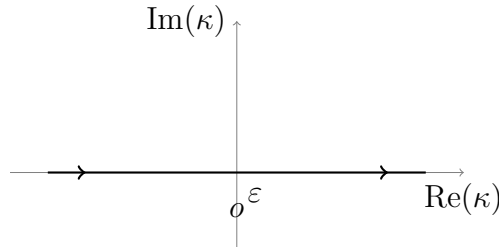
$$\delta^-(\kappa) := \frac{i}{2\pi} \frac{1}{\kappa + i\varepsilon}.$$

In this appendix we want to show the following result:

$$\theta(x) = \int d\kappa e^{-i2\pi\kappa x} \delta^-(\kappa). \tag{20}$$

The term $i\varepsilon$ in the denominator of Equation (20) is nothing but the prescription to follow whenever the integration path runs over a singular point. The integral (20) can be computed remaining on the real axis but moving the singularity on the negative imaginary axis as illustrated in Figure (5). When $x < 0$ we can close the integration contour on the upper

Figure 5: Possible integration path when integrand is $\exp(i2\pi\kappa x)/(\kappa + i\varepsilon)$.



half plane as in Figure (6) and since there is no pole inside the integration path the result is zero. On the other hand, when $x > 0$ we can close the contour in the lower half plane as in Figure (7). Since we are running clockwise the result will be:

$$\begin{aligned} \int d\kappa e^{-i2\pi\kappa x} \delta^-(\kappa) &= \frac{i}{2\pi} \int_{\Gamma} d\kappa e^{-i2\pi\kappa x} \frac{1}{\kappa + i\varepsilon} \\ &= \frac{i}{2\pi} [-2\pi i e^{-i2\pi\kappa(-i\varepsilon)}] = 1 \quad x > 0. \end{aligned}$$

Figure 6: The integration path when integrand is $\exp(-i2\pi\kappa x)/(\kappa + i\varepsilon)$ and $x < 0$.

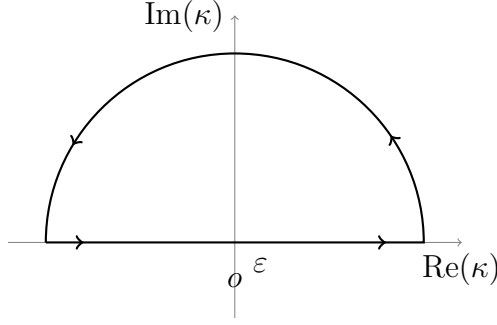
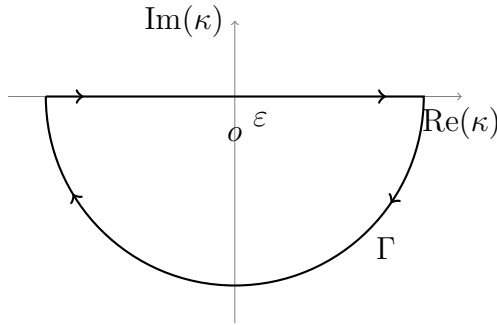


Figure 7: The integration path when integrand is $\exp(-i2\pi\kappa x)/(\kappa + i\varepsilon)$ and $x > 0$.



B The Shannon Sampling Theorem

Let us consider a function $c(x)$ whose domain is centered around the origin, i.e. $c(x): [-X_c, X_c] \rightarrow \mathbb{R}$. Its Fourier transform is defined as

$$\hat{c}(\kappa) = \int_{-X_c}^{X_c} e^{i2\pi\kappa x} c(x) dx,$$

and the Fourier Inversion Theorem guarantees that the original function can be written

$$c(x) = \frac{1}{2X_c} \sum_{n=-\infty}^{\infty} \hat{c}(\kappa_n) e^{-i2\pi\kappa_n x}.$$

An immediate consequence is that

$$\begin{aligned} \hat{c}(\kappa) &= \frac{1}{2X_c} \sum_{n=-\infty}^{\infty} \hat{c}(\kappa_n) \int_{-X_c}^{X_c} e^{i2\pi(\kappa - \kappa_n)x} dx = \frac{1}{2X_c} \sum_{n=-\infty}^{\infty} \hat{c}(\kappa_n) \frac{e^{i2\pi(\kappa - \kappa_n)X_c} - e^{-i2\pi(\kappa - \kappa_n)X_c}}{i2\pi(\kappa - \kappa_n)} \\ &= \sum_{n=-\infty}^{\infty} \hat{c}(\kappa_n) \frac{\sin[2\pi(\kappa - \kappa_n)X_c]}{2\pi(\kappa - \kappa_n)X_c} \\ &= \sum_{n=-\infty}^{\infty} \hat{c}(\kappa_n) \text{sinc}[2\pi(\kappa - \kappa_n)X_c] = \sum_{n=-\infty}^{\infty} \hat{c}(\kappa_n) \text{sinc}[2\pi(\kappa_n - \kappa)X_c], \end{aligned}$$

where we have used that the sinc is an even function, in the last equality.

Similarly, for a function $z(x)$ defined over a bounded interval

$$I_z = \{x : X_l \leq x \leq X_h\},$$

we get back to the same case as above by properly shifting the function z , i.e.

$$c(x) \doteq z(x + X_m), \quad X_m = \frac{X_h + X_l}{2}.$$

Hence, knowledge of this next fact

$$\hat{c}(\kappa_n) = \int_{-X_c}^{X_c} e^{i2\pi\kappa_n x} c(x) dx = e^{-i2\pi\kappa_n X_m} \int_{X_l}^{X_h} e^{i2\pi\kappa_n x} c(x - X_m) dx = e^{-i2\pi\kappa_n X_m} \hat{z}(\kappa_n)$$

makes it not difficult to show that

$$\begin{aligned} \hat{z}(\kappa) &= \int_{X_l}^{X_h} e^{i2\pi\kappa x} z(x) dx = \int_{-X_c}^{X_c} e^{i2\pi\kappa(x+X_m)} z(x + X_m) dx \\ &= e^{i2\pi\kappa X_m} \int_{-X_c}^{X_c} e^{i2\pi\kappa x} c(x) dx = e^{i2\pi\kappa X_m} \hat{c}(\kappa) \\ &= \sum_{n=-\infty}^{\infty} e^{i2\pi\kappa X_m} \hat{c}(\kappa_n) \text{sinc}[2\pi(\kappa_n - \kappa)X_c] \\ &= \sum_{n=-\infty}^{\infty} e^{i2\pi(\kappa - \kappa_n)X_m} \hat{z}(\kappa_n) \text{sinc}[2\pi(\kappa_n - \kappa)X_c], \end{aligned}$$

C The Modified Hilbert Transform

The object of our interest are integrals which take the following form

$$\int \frac{\text{sinc}[a(y - \kappa)]}{\kappa + i\varepsilon} d\kappa = \frac{2\pi}{i} \mathcal{H}^-[\text{sinc}(ay)],$$

that is the Modified Hilbert transform already introduced in Definition 1.

Then

$$\begin{aligned} \mathcal{H}^-[\text{sinc}(ay)] &= \bar{\mathcal{F}}[\mathcal{F}[\text{sinc}(ax)]\mathcal{F}[\delta^-(x)]] \\ &= \frac{\pi}{|a|} \int e^{-i2\pi\kappa y} \theta(-\kappa) \mathbb{1}_{[-\frac{|a|}{2\pi} < \kappa < \frac{|a|}{2\pi}]} d\kappa = \frac{\pi}{|a|} \int_{-\frac{|a|}{2\pi}}^0 e^{-i2\pi\kappa y} d\kappa \\ &= \frac{1}{-2iy|a|} (1 - e^{iy|a|}), \end{aligned}$$

where we make use of the fact that the Fourier transform of the sinc function complies to

$$\begin{aligned}
\mathcal{F}[\text{sinc}(ax)] &= \int e^{i2\pi\kappa x} \frac{\sin(ax)}{ax} dx = \int e^{i2\pi\kappa x} \frac{\sin(ax)}{ax + ai\varepsilon} dx \\
&= \frac{\pi}{a} \int e^{i2\pi\kappa x} \frac{e^{iax} - e^{-iax}}{2\pi i(x + i\varepsilon)} dx = \frac{\pi}{a} \left[\theta\left(\kappa + \frac{a}{2\pi}\right) - \theta\left(\kappa - \frac{a}{2\pi}\right) \right] \\
&= \frac{\pi}{|a|} \mathbb{1}_{[-\frac{|a|}{2\pi} < \kappa < \frac{|a|}{2\pi}]}.
\end{aligned}$$

This is indeed justified by the fact that the sinc function is regular in the origin, so that we can shift the pole everywhere we want on the imaginary axis (and change the contour accordingly) without affecting the integral.

We consequently conclude that our target integral admits solutions of an exponential type

$$\int \frac{\text{sinc}[a(y - \kappa)]}{\kappa + i\varepsilon} d\kappa = \frac{\pi}{y|a|} (1 - e^{iy|a|}).$$

Choosing $a = 2\pi X_c$ and $y = \kappa_n$ finally proves the desired result of Equation (8).

D An Explicit Formulation for the CoN Put Price

This section derives an explicit formulation of the CoN put price, in terms of sin and cos functions multiplying real and imaginary parts of the Fourier transform \hat{f} . So, if we denote $\hat{f}^\dagger(\cdot)$ the complex conjugate of the Fourier transform $\hat{f}(\cdot)$, we immediately have

$$\begin{aligned}
\mathbb{E}[\mathbb{1}_{\{s_T < k\}}] &\simeq \frac{i}{2\pi} \sum_{n=-N/2}^{N/2} e^{-i2\pi k \kappa_n} \hat{f}(\kappa_n) \left[-i\pi \mathbb{1}_{n=0} + \frac{1 - (-1)^n}{n} \mathbb{1}_{n \neq 0} \right] \\
&= \frac{1}{2} + \frac{i}{2\pi} \sum_{n=1}^{N/2} \frac{(1 - (-1)^n)}{n} \left[e^{-i2\pi k \kappa_n} \hat{f}(\kappa_n) - e^{i2\pi k \kappa_n} \hat{f}^\dagger(\kappa_n) \right],
\end{aligned}$$

which can be rewritten as

$$= \frac{1}{2} + \frac{i}{\pi} \sum_{n=1}^{N/4} \frac{1}{2n-1} \left[e^{-i2\pi k \kappa_{2n-1}} \hat{f}(\kappa_{2n-1}) - e^{i2\pi k \kappa_{2n-1}} \hat{f}^\dagger(\kappa_{2n-1}) \right].$$

Properly rearranging terms based on Euler's formula, we obtain

$$\begin{aligned}
\mathbb{E}[\mathbb{1}_{\{s_T < k\}}] &\simeq \frac{1}{2} - \frac{2}{\pi} \sum_{n=1}^{N/4} \frac{1}{2n-1} \left[\cos(2\pi k \kappa_{2n-1}) \Im[\hat{f}(\kappa_{2n-1})] + \right. \\
&\quad \left. - \sin(2\pi k \kappa_{2n-1}) \Re[\hat{f}(\kappa_{2n-1})] \right].
\end{aligned}$$

E Numerical Moments of q -th Order

The computation of the moments of a distribution requires to manage integrals which are not always ensured to admit a closed form solution. Nevertheless, the knowledge of the CF allows to evaluate them numerically. This fact is of crucial importance if one wants to truncate the PDF according to the cumulants-based rule of Fang and Oosterlee (2009) but should be clearly recognized to have a much wider scope. That is why we suppress dependence on s_T and talk about a random variable X defined over the support $[-X_c, X_c]$, in this section.

Let us first recall the next fundamental relation between the q -th order moment of X and its CF ϕ_X :

$$\mathbb{E}[X^q] = (i2\pi)^{-q} \frac{d^q}{d\kappa^q} \phi_X(\kappa) \Big|_{\kappa=0}$$

then, if we apply the Shannon Sampling Theorem

$$= (i2\pi)^{-q} \sum_{n=-\infty}^{\infty} \phi_X(\kappa_n) \frac{d^q}{d\kappa^q} \text{sinc}(2\pi(\kappa_n - \kappa)X_c) \Big|_{\kappa=0}$$

and perform a simple change of variable, we have

$$= (iX_c)^q \sum_{n=-\infty}^{\infty} \phi_X(\kappa_n) \frac{d^q}{dt^q} \text{sinc}(t) \Big|_{t=n\pi}. \quad (21)$$

Furthermore, a power series expansion of the sinc function, i.e.

$$\text{sinc}(t) = \sum_{n=0}^{\infty} (-1)^n \frac{t^{2n}}{(2n+1)!}$$

is readily obtained given the corresponding expansion for the sin function, and this clearly justifies a number of properties. Among them we have the following:

- odd derivatives are such that
- terms of the following type

$$\frac{d^{2q+1}}{dt^{2q+1}} \text{sinc}(t) \Big|_{t=0} = 0$$

by parity of the sinc function

$$\frac{d^{2q+1}}{dt^{2q+1}} \text{sinc}(t) \Big|_{t=n\pi}$$

are odd with respect to n

- even derivatives are such that
- terms of the following type

$$\left. \frac{d^{2q}}{dt^{2q}} \text{sinc}(t) \right|_{t=0} = \frac{(-1)^q}{2q+1} \quad \left. \frac{d^{2q}}{dt^{2q}} \text{sinc}(t) \right|_{t=n\pi}$$

by the theory of Taylor series

are even with respect to n

These properties play a fundamental role when specifying Equation (21) for some given q .

We report the explicit formulation of the first few moments next:

$$\begin{aligned} m_1 &= \mathbb{E}[X] = -2X_c \sum_{n=1}^{\infty} \Im[\phi_X(\kappa_n)] \frac{(-1)^n}{n\pi}, \\ m_2 &= \mathbb{E}[X^2] = \frac{X_c^2}{3} + 4X_c^2 \sum_{n=1}^{\infty} \Re[\phi_X(\kappa_n)] \frac{(-1)^n}{(n\pi)^2}, \\ m_3 &= \mathbb{E}[X^3] = -2X_c^3 \sum_{n=1}^{\infty} \Im[\phi_X(\kappa_n)] \left[\frac{(-1)^n}{n\pi} \left(1 - \frac{6}{(n\pi)^2} \right) \right], \\ m_4 &= \mathbb{E}[X^4] = \frac{X_c^4}{5} + 8X_c^4 \sum_{n=1}^{\infty} \Re[\phi_X(\kappa_n)] \left[\frac{(-1)^n}{(n\pi)^2} \left(1 - \frac{6}{(n\pi)^2} \right) \right]. \end{aligned}$$

F Error Analysis (proof)

The overall error ϵ is equal to the sum $\epsilon_1 + \epsilon_2 + \epsilon_3$ and its norm can be bounded as

$$|\epsilon| \leq \epsilon_1 + |\epsilon_2| + |\epsilon_3|.$$

Arguing in the same way as in the COS paper, ϵ_1 can be made arbitrarily small by choosing a sufficiently high value for X_c . As far as ϵ_2 is concerned, it is clear from Equation (7) that it corresponds to the remainder of a series converging to $\mathbb{E}[\mathbb{1}_{\{s_T < k\}} \mathbb{1}_{\{-X_c \leq s_T \leq X_c\}}]$. Then, when N increases, ϵ_2 goes to zero⁹.

Concerning ϵ_3 , one has

$$|\epsilon_3| \leq \frac{1}{\pi} \sum_{n=-N/4}^{N/4} \frac{1}{|2n-1|} \left| \overbrace{f \mathbb{1}_{\{-X_c \leq s_T \leq X_c\}}(\kappa_{2n-1})} - \hat{f}(\kappa_{2n-1}) \right|.$$

⁹It is possible to derive an analytic bound for ϵ_2 , assuming some mild regularity for the PDF. The reasoning is similar to that in Fang and Oosterlee (2009).

To bound the last quantity, we can proceed following two strategies, which are based upon different assumptions. We first recall that

$$\hat{f}(\kappa_{2n-1}) - \overline{f \mathbb{1}_{\{-X_c \leq s_T \leq X_c\}}}(\kappa_{2n-1}) = \int_{\mathbb{R} \setminus [-X_c, X_c]} f(s_T) e^{i2\pi\kappa_{2n-1}s_T} ds_T.$$

To ensure convergence of AoN and PV call prices, for $s_T \gg 1$ the PDF $f(s_T)$ has to satisfy

$$f(s_T) \leq C e^{-\beta s_T},$$

with $C > 0$ and $\beta > 1$. For $s_T \ll -1$, we assume the following condition – typically satisfied by commonly used stochastic models for log-returns

$$f(s_T) \leq C e^{\gamma s_T},$$

with $\gamma > 0$. Then,

$$\begin{aligned} |\epsilon_3| &\leq \frac{1}{\pi} \sum_{n=-N/4}^{N/4} \frac{1}{|2n-1|} \left| \int_{\mathbb{R} \setminus [-X_c, X_c]} f(s_T) e^{i2\pi\kappa_{2n-1}s_T} ds_T \right| \\ &\leq \frac{1}{\pi} \sum_{n=-N/4}^{N/4} \frac{1}{|2n-1|} \int_{\mathbb{R} \setminus [-X_c, X_c]} f(s_T) ds_T \leq \frac{2}{\pi} \sum_{n=0}^{N/4} \frac{1}{2n+1} \int_{\mathbb{R} \setminus [-X_c, X_c]} f(s_T) ds_T \\ &\leq \frac{1}{\pi} (2 + \log(N/2 + 1)) \int_{\mathbb{R} \setminus [-X_c, X_c]} f(s_T) ds_T \\ &\leq \frac{C}{\pi} (2 + \log(N/2 + 1)) \left(\frac{1}{\gamma} e^{-\gamma X_c} + \frac{1}{\beta} e^{-\beta X_c} \right). \end{aligned}$$

Naming $\delta = \min(\beta, \gamma) > 0$, we obtain

$$|\epsilon_3| \leq \frac{C}{\pi} (2 + \log(N/2 + 1)) e^{-\delta X_c}.$$

To conclude, it is sufficient to choose X_c proportional to $\log(N/2 + 1)$. Practically, this assumption amounts to choose L proportional to $\log(N/2 + 1)$ in (6). Then, ϵ_3 can be made arbitrarily small by increasing N .

An alternative strategy allows to reach the same conclusion, without assuming the dependence of X_c on N , but under a different hypothesis about the asymptotic behavior of the density $f(s_T)$. We can split the integral $\int_{\mathbb{R} \setminus [-X_c, X_c]} f(s_T) e^{i2\pi\kappa_{2n-1}s_T} ds_T$ in two terms, I_1 and I_2 , with

$$I_1(\kappa_{2n-1}) = \int_{-\infty}^{-X_c} f(s_T) e^{i2\pi\kappa_{2n-1}s_T} ds_T \quad \text{and} \quad I_2(\kappa_{2n-1}) = \int_{X_c}^{+\infty} f(s_T) e^{i2\pi\kappa_{2n-1}s_T} ds_T,$$

so that

$$|\epsilon_3| \leq \frac{1}{\pi} \sum_{n=1}^{N/4} \frac{1}{2n-1} |I_1(\kappa_{2n-1}) + I_2(\kappa_{2n-1})| + \frac{1}{\pi} \sum_{n=1}^{N/4} \frac{1}{2n+1} \left| I_1^\dagger(\kappa_{2n+1}) + I_2^\dagger(\kappa_{2n+1}) \right|. \quad (22)$$

Let us consider $I_2(\kappa_{2n-1})$ and define the variable y via the relation

$$s_T = y + \frac{X_c}{2n-1}.$$

Then,

$$\begin{aligned} I_2(\kappa_{2n-1}) &= - \int_{X_c - X_c/(2n-1)}^{+\infty} e^{i2\pi\kappa_{2n-1}y} f\left(y + \frac{X_c}{2n-1}\right) dy \\ &= - \int_{X_c}^{+\infty} e^{i2\pi\kappa_{2n-1}y} f\left(y + \frac{X_c}{2n-1}\right) dy - \int_{X_c - X_c/(2n-1)}^{X_c} e^{i2\pi\kappa_{2n-1}y} f\left(y + \frac{X_c}{2n-1}\right) dy. \end{aligned}$$

It follows that

$$\begin{aligned} I_2(\kappa_{2n-1}) &= \frac{1}{2} \int_{X_c}^{+\infty} e^{i2\pi\kappa_{2n-1}y} \left(f(y) - f\left(y + \frac{X_c}{2n-1}\right) \right) dy \\ &\quad - \frac{1}{2} \int_{X_c - X_c/(2n-1)}^{X_c} e^{i2\pi\kappa_{2n-1}y} f\left(y + \frac{X_c}{2n-1}\right) dy \end{aligned}$$

so

$$|I_2(\kappa_{2n-1})| \leq \frac{1}{2} \int_{X_c}^{+\infty} \left| f(y) - f\left(y + \frac{X_c}{2n-1}\right) \right| dy + \frac{1}{2} \int_{X_c - X_c/(2n-1)}^{X_c} f\left(y + \frac{X_c}{2n-1}\right) dy.$$

We now assume that $f(s_T)$ is monotonically convergent to zero for sufficiently large $|s_T|$.

The argument of the modulus is positive, so

$$|I_2(\kappa_{2n-1})| \leq \frac{1}{2} \int_{X_c}^{X_c(1+\frac{1}{2n-1})} f(s_T) ds_T + \frac{1}{2} \int_{X_c}^{X_c(1+\frac{1}{2n-1})} f(s_T) ds_T \leq \frac{X_c}{2n-1} f(X_c).$$

Defining $s_T = y - X_c/(2n-1)$, it readily follows that

$$|I_1(\kappa_{2n-1})| \leq \frac{X_c}{2n-1} f(-X_c).$$

Similar results hold for $I_1^\dagger(\kappa_{2n+1})$ and $I_2^\dagger(\kappa_{2n+1})$.

From Equation (22), we obtain

$$|\epsilon_3| \leq \frac{X_c}{\pi} (f(X_c) + f(-X_c)) \sum_{n=1}^{N/4} \left(\frac{1}{(2n-1)^2} + \frac{1}{(2n+1)^2} \right)$$

and, based on the following observation¹⁰

$$\sum_{n=1}^{\infty} \left(\frac{1}{(2n-1)^2} + \frac{1}{(2n+1)^2} \right) = \frac{\pi^2}{4} - 1$$

we write

$$|\epsilon_3| \leq \frac{X_c}{\pi} (f(X_c) + f(-X_c)) \Upsilon,$$

where Υ is a moderate constant (certainly smaller than $\pi^2/4 - 1$).

To conclude, it is sufficient to assume the existence of the first moment of s_T . Indeed, this implies that $f(s_T) = o(1/s_T)$ for $|s_T| \rightarrow +\infty$. Then, $X_c f(X_c)$ and $X_c f(-X_c)$ can be made arbitrarily small by choosing X_c sufficiently large.

G The Fractional Fourier Transform

Throughout this paper we had to compute double infinite sums of the type:

$$p(x) = \frac{1}{2X_c} \sum_{n=-\infty}^{+\infty} \hat{p}_n e^{-i2\pi k_n x} \quad 0 \leq x \leq 2X_c, \quad \text{with} \quad k_n = \frac{n}{2X_c}$$

The p_N approximation to $p(x)$ is given by:

$$p_N(x) = \frac{1}{2X_c} \sum_{n=-N/2}^{N/2} \hat{p}_n e^{-i2\pi k_n x}.$$

If we confine our interest to the discrete set of values:

$$x_m = m \frac{2X_c}{N}, \quad -N/2 \leq m < N/2$$

we get:

$$p_N(x_m) = \frac{1}{2X_c} \sum_{n=0}^{N-1} \hat{q}_n e^{-i2\pi n m/N}$$

¹⁰We thank an anonymous referee for pointing this out.

$$q_n = \begin{cases} p_n & 0 \leq n < N/2, \\ p_{N/2} + p_{-N/2} & n = N/2, \\ p_{n-N} & N/2 < n < N. \end{cases}$$

and this sum is what we compute with the FFT.

The fractional Fourier transform computes:

$$p_N(\hat{x}_m) = \frac{1}{2X_c} \sum_{n=-N/2}^{N/2-1} \hat{p}_n e^{-i2\pi nm\epsilon/N}.$$

where $\hat{x}_m = m\epsilon\delta x$.